Clouds and the Earth's Radiant Energy System (CERES)

Algorithm Theoretical Basis Document

Overview of Cloud Retrieval and Radiative Flux Inversion

(Subsystem 4.0)

B. A. Wielicki[1]
B. A. Baum[1]
J. A. Coakley, Jr.[2]
R. N. Green[1]
Yongxiang Hu[3]
M. D. King[4]
Bing Lin[3]
D. P. Kratz[1]
P. Minnis[1]
L. L. Stowe[5]

[1]Atmospheric Sciences Division, NASA Langley Research Center, Hampton, Virginia 23681-0001
[2]College of Oceanic & Atmospheric Sciences, Oregon State University, Corvallis, OR 97331-2209
[3]Hampton University, Hampton, Virginia 23668
[4]Earth Sciences Directorate, Goddard Space Flight Center, Greenbelt, MD 20771
[5]National Oceanic and Atmospheric Administration Science Center, Washington, DC 20233

June 2, 1997

CERES Top Level Data Flow Diagram

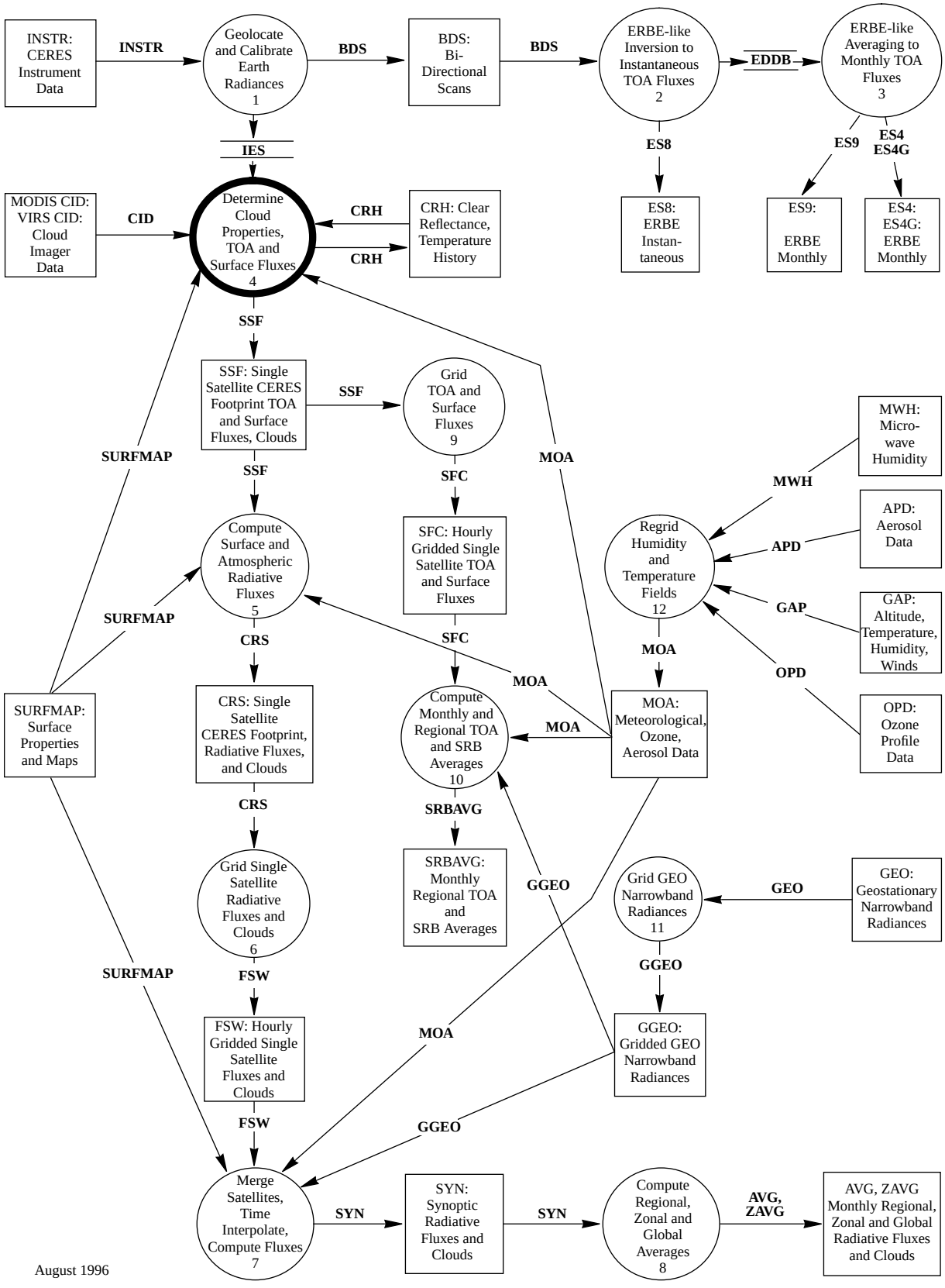

Subsystem 4.0 Top Level Data Flow Diagram

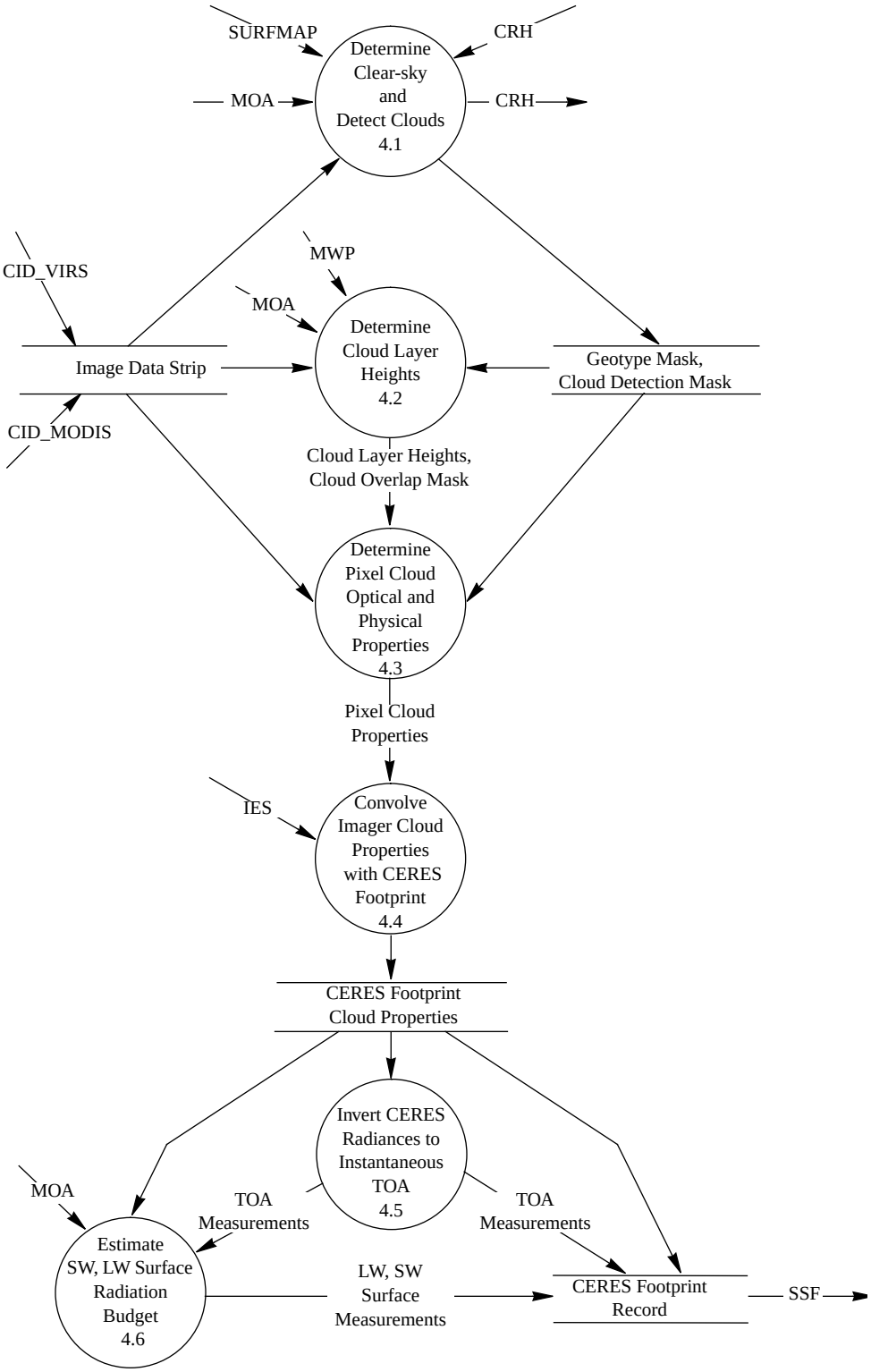

Abstract

One of the major advances of the CERES (Clouds and the Earth's Radiant Energy System) radiation budget analysis over the ERBE (Earth Radiation Budget Experiment) is the ability to use high spectral and spatial resolution cloud imager data to determine cloud and surface properties within the relatively large CERES field of view [20-km diameter for the Earth Observing System (EOS)-AM and EOS-PM, 10 km diameter for TRMM (Tropical Rainfall Measuring Mission)]. For the first launch of the CERES broadband radiometer on TRMM in 1997, CERES will use the VIRS (Visible Infrared Scanner) cloud imager as input. For the next launches on EOS-AM (1998) and EOS-PM (2000), CERES will use the MODIS (Moderate-Resolution Imaging Spectroradiometer) cloud imager data as input.

This overview summarizes the Subsystem 4 CERES algorithms which

1. *Determine clear-sky radiances and detect pixels containing clouds*
2. *Determine well-defined cloud layers and identify multilayer pixels*
3. *Determine cloud properties for each imager pixel*
4. *Map the imager cloud properties to the CERES broadband radiance footprint*
5. *Use the CERES footprint cloud properties to determine an angular distribution model for the conversion of radiance to top-of-atmosphere (TOA) flux*
6. *Use the TOA fluxes and parameterizations to estimate surface radiative fluxes*

Angular sampling errors were determined to be the largest error source for ERBE shortwave fluxes. The increased accuracy of CERES cloud property determination and the new angular models are expected to reduce these errors by a factor of 3 to 4. The cloud properties and radiative fluxes for each CERES footprint are also key to providing more accurate estimates of in-atmosphere radiative fluxes. These in-atmosphere radiative flux calculations are discussed in Subsystem 5.

4.0. Overview of Cloud Retrieval and Radiative Flux Inversion

4.0.1. Introduction

This documentation is intended as an overview of the CERES subsystems which produce the SSF data product of instantaneous TOA radiative fluxes, surface radiative fluxes, and cloud properties. Because of its complexity the cloud retrieval algorithm is broken into 3 subsystems. The primary purpose of this document is to overview the connectivity and assumptions of these three cloud subsystems (4.1, 4.2, 4.3). Subsystems 4.4-4.6 are relatively self-contained and are dealt with primarily within each specific subsystem document. The cloud retrieval algorithm has two major objectives.

The first objective is to derive surface and cloud properties sufficient to classify a unique set of targets with distinctly different anisotropic radiation fields. This is required so that the CERES rotating

azimuth plane scanner can observe a complete range of surface and cloud targets for all typical viewing and solar angle geometries for a given satellite orbital geometry. These cloud determinations are then combined with the CERES broadband scanner radiance data to derive empirical models of shortwave (SW) and longwave (LW) anisotropy required to accurately convert the CERES-measured radiances into unbiased estimates of radiative fluxes. For example, we would combine observations of boundary layer cumulus with cloud fractions between 20 and 30% over a tropical forest background. In turn, this cumulus cloud class might further be broken into several optical depth classes. In this manner, even the potentially large but uncertain effect of 3-D cloud structure can be implicitly included in the anisotropic models. Testing of these concepts has begun by using the Nimbus-7 THIR (Temperature-Humidity Infrared Radiometer) and TOMS (Total Ozone Mapping Spectrometer) cloud properties (Stowe et al. 1988) and ERB (Earth Radiation Budget) broadband radiances (Jacobowitz et al. 1984), as well as using the Release 1 CERES cloud algorithm using AVHRR (Advanced Very High Resolution Radiometer), HIRS (High-Resolution Infrared Sounder), and ERBE global radiance data sets.

The second objective is to provide a set of cloud properties optimally designed for studies of the role of clouds in the Earth's radiation budget. In particular, cloud properties determined using high spatial (0.25–2 km at nadir) and spectral resolution cloud imager data will be matched to each CERES footprint (10–20 km at nadir) to as consistently as possible tie the cloud physical and cloud broadband radiative properties. These cloud properties will be used in calculations of the surface and in-atmosphere radiative fluxes. Because all current cloud remote sensing methods use 1-D radiative transfer models, which are not appropriate for optically thick cumulus clouds, the close tie of CERES TOA fluxes to imager cloud properties allows a first-order correction for 3-D cloud effects. For example, TOA reflected SW flux computed using the 1-D-determined imager cloud optical depth and cloud particle size may differ greatly from the observed TOA flux. The observed flux used empirical models of cloud anisotropy to correctly convert radiance into flux even for 3-D cloud structure. This flux can then be used to determine an "equivalent" plane-parallel cloud optical depth or to specify a 3-D cloud parameter such as cloud aspect ratio. In this sense, the CERES cloud algorithm will produce an initial estimate of cloud properties. This estimate will then be modified to obtain consistency in cloud properties and TOA broadband radiative fluxes. This consistency will be essentially that required to examine global climate models, which use 1-D radiative flux computations similar to those performed by CERES.

4.0.2. Input and Output Data

The primary input data sets for Subsystem 4 are the CERES broadband radiance data and the cloud imager data. Other auxiliary input data sets are discussed more fully in Subsystems 4.1–4.3 and in the input data descriptions in appendix A. The CERES instrument data are described in Subsystem 1. The cloud imager data vary between prelaunch studies, TRMM, and EOS, and a brief overview is given below.

VIRS is a next generation version of the AVHRR scanning radiometer with a 2-km diameter nadir field of view and five spectral channels (0.65, 1.6, 3.75, 10.8, and 12.0 μm). The major advances over the current AVHRR are the addition of a 1.6-μm channel and onboard solar channel calibration. The AVHRR instrument has shown large changes in instrument gain with time (Staylor, 1990; NESDIS, 1993).

MODIS (King et al. 1992) will be a major improvement over both AVHRR and VIRS. Onboard calibration will be greatly improved for solar reflectance channels by including onboard lamps, solar diffuser plate, and especially by the ability to use the moon as a stable target. Channel spectral wavelengths will also be monitored in flight. MODIS provides 11 spectral channels of prime use for cloud analysis, including

- 13.3, 13.6, and 13.9 μm for determining thin cirrus cloud height
- 1.38 μm for detecting very thin cirrus, even in the presence of low cloud

- 3.7, 8.5, 11, and 12 μm for determining nighttime cloud particle size/phase
- 0.65, 1.6, and 2.1 μm for determining daytime optical depth, particle size/phase

The thermal infrared channels have a field of view diameter of 1 km, the near infrared are 0.5 km, and the visible channel is 0.25 km. The high spatial resolution visible channel eliminates the problem of partially cloud filled fields of view even for boundary layer clouds such as cumulus (Wielicki and Parker, 1992).

The CERES cloud retrieval algorithm will use the cloud imager data to produce estimates of basic cloud physical and optical properties within each CERES footprint including

- Fractional coverage
- Temperature/height/pressure
- Optical depth (0.65 μm)
- Emissivity (11 μm)
- Particle size and phase
- Liquid/ice water path
- Vertical thickness
- Vertical aspect ratio

The cloud properties are listed roughly in the order of expected accuracy and current understanding of their retrieval. The first four properties are reasonably well understood, the next two are in advanced stages of development, and the last two are only in the beginning stages of development, and may only provide useful information for a limited range of cloud conditions. These properties cover a reasonably complete set of variables to describe the effect of clouds on the radiative fluxes at the surface, within the atmosphere, and at the top of the atmosphere. They are not a rigorously exhaustive set. For example, cloud vertical aspect ratio is a variable which is intended (along with cloud fraction and cloud optical depth) to allow at least a limited investigation of the effects of 3-D radiative transfer issues.

Surface observers indicate that about half of cloud observations are multilayered (Warren et al. 1985), and that multilayered clouds are much more likely over ocean than land. Over ocean, 52% of all observations are multilayered while 43% are single-layered. Over land, 31% are multilayered while 47% are single-layered. Tian and Curry (1989) used the combined satellite, aircraft, and surface cloud observations in the Air Force 3DNEPH data to examine cloud overlap assumptions over the North Atlantic Ocean, and concluded that for cloud layers within 1 km in altitude, maximum overlap is most accurate, while for cloud altitudes separated by 3 km or more, random overlap is the best assumption. Their study further concluded that at a spatial scale of 45 km (similar to the CERES footprint) 75% of the multilayered cases consisted of two-layer cloud systems. As the spatial scale of interest increases to 220 km, three-layer cases dominate. We conclude that the CERES cloud analysis must commonly address the issue of two-layer cloud systems.

All current global satellite cloud climatologies assume a single cloud layer to occur in each imager pixel, although multiple cloud layers are allowed in large regions. For example, subtropical optically thin cirrus overlying a lower boundary layer cloud gives cloud height properties dominated by the cold cirrus and cloud optical depth dominated by the optically thicker stratus cloud. Recent studies of the sensitivity of the LW surface radiation budget to cloud overlap assumptions show that knowledge of cloud overlap is more important than accurate knowledge of the thickness of individual cloud layers (Subsystem 5.0).

CERES will employ two strategies to improve the remote sensing of multilayer clouds. For an optically thin high cloud over low clouds, the MODIS CO_2 sounding channels will be used to establish the upper cloud height and optical depth, while the spectral window visible and infrared channels will be

used for the low clouds (Baum et al. 1994). For an optically thick high cloud over a low cloud, the cloud imager channels will be used for the high cloud properties, while passive microwave liquid water path (LWP) measurement (Greenwald et al. 1993) is used to indicate the presence of the lower cloud layer over ocean backgrounds. These two improvements for sensing multilevel clouds should provide substantially better estimates of LW surface and in-atmosphere radiation budget.

4.0.3. Algorithm Assumptions

Any algorithm to remotely sense physical or radiative properties is based on an assumed physical model. This conceptual model may be explicit (plane-parallel radiative calculations) or implicit (piecewise constant spatial averaging). The more explicit the conceptual model, the more precisely the algorithm strengths and weaknesses can be understood. This is particularly the case in validating the algorithm results. The most fruitful validation is not simply the comparison of end results, but rather the validation of underlying assumptions. The successes and failures of these assumptions lead to critical new results and methods.

The CERES cloud identification and radiative flux determination algorithms are currently based on the following assumptions.

1. ***Cloud-filled pixel assumption: Clouds are much larger than a cloud imager pixel, so that cloud cover in a pixel is 0 or 1.***

This assumption is the subject of much debate. While no data have conclusively answered this question, initial answers are beginning to arrive. The cloud types most subject to error are those with the smallest cloud cells such as cumulus. Figure 4.0-1 shows the accuracy of detecting oceanic boundary layer cloud amount with different spatial resolution sensors (4, 2, 1, 0.5, 0.25, and 0.125 km diameter optical field of view). The results are an extension of the results of Wielicki and Parker (1992) to a much larger number of cases. The results shown here are for 52 cloud fields (each 58.4 km square), but show similar results to those found earlier, although now the bias can be shown to be a systematic function of cloud amount.

Each point in the scatter plot gives the regional cloud fraction in one of the 58.4-km regions. Note that the current ISCCP (International Satellite Cloud Climatology Project) data use 4–8 km resolution data, depending on the satellite [GOES (Geostationary Operational Environmental Satellite) is 8 km, GMS (Geosynchronous Meteorological Satellite) and METEOSAT are 5 km, and AVHRR is 4 km]. Figure 4.0-1 shows that the maximum “beam filling” error is at a cloud amount of 0.5, where partially cloud-filled pixels are sufficiently bright to trigger the cloud threshold, but are treated as cloud filled. For cloud amounts less than about 0.2, the large pixel data underestimate cloud amount, since few of the pixels have sufficient cloud cover to exceed the cloud threshold.

For 4-km data, average cloud fraction for the 52 cases is biased too large by 0.06, with a 1σ rms error of about 0.11. The use of VIRS 2-km data reduces this error by about 30% to 0.04 bias and 0.08 (1σ). The 0.5 km and 0.25 km results typical of MODIS resolution show a small bias of about –0.02 and 1σ of 0.04. The bias for these last two cases is dominated by the difference in reflectance threshold between the reference data (Rclr + 1.5%) and the ISCCP radiance threshold, which for the cases here is equivalent to approximately Rclr + 4.5%, where Rclr is the nadir bidirectional reflectance as defined in Wielicki and Parker (1992). Given very high spatial resolution data, the ISCCP threshold misses significant amounts of optically thin clouds, even for boundary layer clouds. Note that for these cases, the reference threshold would detect a cloud with 10-μm water droplets at a visible optical depth of about 0.3. If the reflectance threshold of the 0.125-km pixel analysis is set equal to the reference case, the two agree to better than 0.01 in cloud fraction. We conclude that the MODIS 0.25-km visible channel is sufficient to derive cloud cover for oceanic boundary layer clouds with errors of a few percent or less.

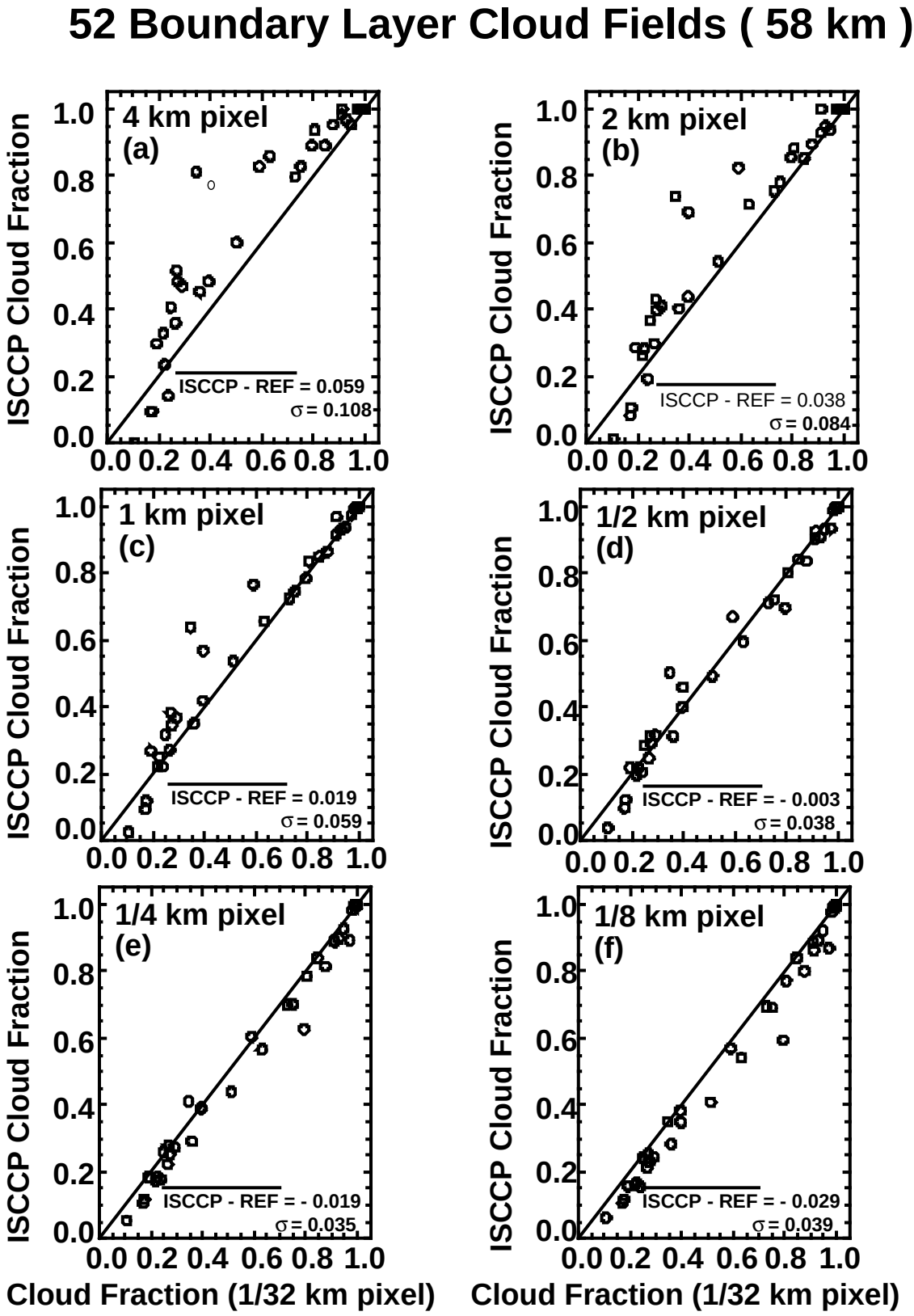

Figure 4.0-1. Effect of sensor spatial resolution on ISCCP threshold estimate of boundary layer cloud fraction. Reference is 57-m spatial resolution Landsat data. All pixel sizes are diameter of the optical field of view. Each point represents cloud fraction for a 58-km region.

Cirrus clouds have also been examined using numerous Landsat scenes. For cirrus, the thermal threshold dominates, so that the MODIS 1-km and VIRS 2-km resolutions are pertinent to the CERES algorithm. Figure 4.0-2 gives a similar result for cirrus cloud fields. As in Wielicki and Parker (1992), the cirrus clouds show very little spatial resolution effects for pixel sizes of 1–8 km. We conclude that the cloud-filled pixel assumption is reasonable for AVHRR, VIRS, and MODIS for cirrus clouds. While these results are encouraging, further work is needed, especially for land cumulus. Studies to verify the accuracy of this approximation are underway using cumulus cloud fields over the Amazon.

The most difficult problem may be the detection of boundary layer clouds at night, when even the MODIS retrievals will require the use of 1-km data. The thermal contrast of these clouds at night is much less than the visible reflectance contrast during the day. The problem of missing optically thin clouds may become more severe. Verification of the accuracy of nighttime detection must be performed with coincident lidar and cloud imager data, or with very high spatial resolution data from the MAS (MODIS Airborne Simulator) on the ER-2 aircraft, or ASTER on the EOS-AM platform.

2. Independent pixel assumption: Clouds can be modeled as plane-parallel, even though they exhibit large horizontal variability in optical depth.

An excellent discussion of this assumption can be found in Cahalan et al. (1994). They demonstrate that the assumption is accurate to a few percent for narrowband flux calculations with overcast marine boundary layer clouds. Wielicki and Parker (1992) found support for the plane-parallel assumption using Landsat nadir radiances at 0.83 μm and 11 μm for broken and solid boundary layer clouds. Stackhouse and Stephens (1994) found rms errors of up to 20% in derived optical depths using plane-parallel radiance calculations, although bias errors were much smaller. More recently Loeb et.al. (1997) found discrepancies in forward and backward scattered radiance measurements by AVHRR of 10 to 20%. In general, this assumption will be less accurate for radiances than for fluxes.

Chambers et al. (1996) tested the internal consistency of Landsat derived cloud optical depth for the boundary layer cloud cases used in Fig 4.0-3. The apparent horizontal variability in the cloud fields observed at the Landsat 30 m spatial scale were used as input to a 2-D (horizontal/vertical) radiative transfer model. The 2-D model is then used to verify the differences in cloud optical depth inferred using full 2-D radiance solutions versus 1-D IPA radiance solutions. The results depended on spatial scale and solar zenith angle. For individual 30 meter Landsat pixels, the difference between 2-D and 1-D inferred optical depth gave standard deviations of 100% of the mean value for cumulus clouds, 50% for broken stratocumulus, and 10% for overcast stratocumulus. For 58 km regional averages more typical of a CERES field of view, however, the standard deviations dropped to 10-25%, 10-19%, and 2% respectively, where larger errors are for overhead sun conditions. Bias errors ranged from 3-15% for cumulus, 1-10% for broken stratocumulus, and 3% for overcast conditions. The Chambers et.al. (1996) results were calculated using flat topped boundary layer clouds, while the Loeb et.al. (1997) results indicate that variable cloud top height will significantly increase these errors.

The relatively small errors of this assumption seem to be caused by three properties of the clouds examined:

- A red spectrum of radiance variability, typical of most meteorological fields. This means that as spatial scale decreases, cloud optical property variability decreases. A red spectrum limits the “sharpness” of cloud edges.
- Low to moderate optical depths for the cirrus and marine boundary layer clouds, especially for broken clouds (Harshvardhan et al. 1994; Wielicki and Parker, 1992; Luo et al. 1994). Welch et al. (1980) used Monte Carlo radiative model calculations to show that the effect of horizontal inhomogeneity on fluxes became pronounced only for cloud optical depths above about 8. Most of the cirrus and broken marine boundary layer clouds appear to be at lower optical depths, thereby minimizing the effects.

- Cloud vertical aspect ratios (vertical/horizontal) are typically much less than 1 for cirrus and inversion-capped boundary layer clouds.

The most severe test of this assumption will come with examination of boundary layer cumulus over land (Wielicki and Welch, 1986), and deep convection over land and ocean, which will have large optical depths and large aspect ratios. One of the complications caused by deep convection, or any high optically thick cloud with sharp edges, is the problem of cloud shadowing. Subsystem 4.3 discusses the effect of shadowing on cloud optical property retrieval and suggests strategies for minimizing the effect.

Even if the independent pixel assumption is without error, Cahalan et al. (1994), Stephens (1988), and Barker et al. (1996) showed that optical depths cannot be spatially or temporally averaged without causing large errors in radiative flux calculations. This error is simply caused by the nonlinear relationship between albedo and optical depth. CERES cloud retrievals will minimize this problem by saving 1-D histograms of cloud visible (0.65 μm) optical depth calculated using the highest resolution cloud imager data available (Subsystem 4.5). These histograms will be carried through the spatial gridding and time averaging processes as well as averaging to instantaneous CERES footprints. One step to minimize this error is to average $\ln(\tau)$ as opposed to a linear average of τ (Rossow et al. 1991). The advantage of this process is that cloud spherical albedo is roughly linear in $\ln(\tau)$, so that this variable comes closer to conserving the cloud albedo. In fact, the errors showed by Cahalan et al. (1994) would have been significantly reduced if this averaging had been used.

Although we discussed the impact of the cloud-filled pixel assumption on cloud fraction, what is its impact on cloud optical depth? Figure 4.0-3 shows the effect of varying pixel size on the derived average optical depth in the 58.4 km region. The results shown are for linear-averaged optical depth, and therefore are more typical of spatially averaged error in LWP which for a fixed cloud particle size is linear in optical depth (Subsystem 4.3). For 4-km pixels, the bias error is an underestimate of 23%, with a 1σ of 25%. The fractional error is much larger than cloud amount errors because the spatial averaging error discussed above (using a spatially averaged reflectance) will always underestimate the true average optical depth (Cahalan et al. 1994) and the cloud filled-pixel error (clear regions in cloudy pixels lower the mean reflectance) will also underestimate the optical depth. For the 2-km VIRS data, the error drops to a bias of 16%, while finally for 0.25-km data, the bias becomes an overestimate of 2% with a 1σ of 9%. Why the overestimate for small pixels? This shows the effect of changing from the reference threshold at Rclr + 1.5% to the ISCCP value of approximately Rclr + 4.5%. The ISCCP threshold misses some of the optically thin clouds picked up by the smaller threshold. This is confirmed by the fact that the bias is largest for the smallest optical depth clouds.

A similar analysis of optical depth errors was carried out for the cirrus cloud fields used in Fig. 4.0-2. Optical depth retrievals were carried out using the hexagonal ice crystal scattering phase functions (Takano and Liou, 1989) for both the ISCCP and reference (i.e. full resolution) results. In this way, we isolate errors caused by spatial resolution effects, or by cloud threshold effects. For cirrus analysis using 4-km pixels, the bias errors in optical depth for 58.4 km regions (ISCCP - reference) were -0.5% with a standard deviation of 13%. For the VIRS pixel size of 2 km, bias errors were 4% with a standard deviation of 9%. For the MODIS pixel size of 0.25 km, bias errors were 4%, with a standard deviation of 8%. As for the earlier boundary layer results, bias errors at high spatial resolution such as MODIS are dominated by the different cloud detection thresholds used in the reference and ISCCP detection algorithms. The results indicate no significant sensitivity of derived cirrus optical depth to sensor spatial resolution for fields of view less than 2 km, and only a small effect even for 8 km fields of view.

Further studies are needed to examine the errors for logarithmic averaging of optical depth, and the determination of optimal thresholds as a function of spatial resolution. Finally, as discussed by Stephens (1988) and Rossow (1989), the optimal methods for spatial and temporal averaging of cloud physical and optical properties have yet to be established. CERES will perform studies using the broadband radiative models discussed in Subsystem 5 along with imager pixel-level cloud properties to examine the

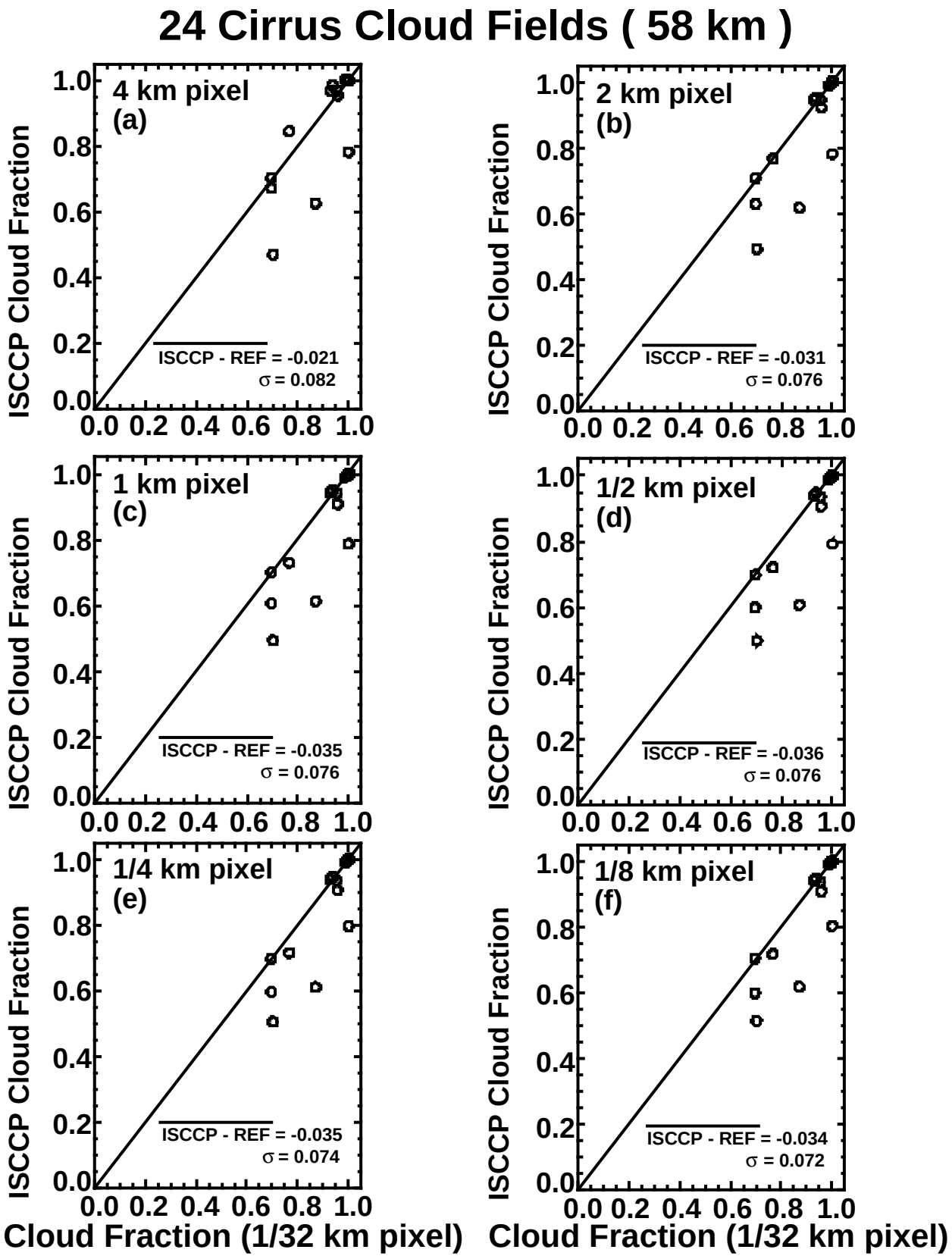

Figure 4.0-2. Effect of sensor spatial resolution on ISCCP threshold estimate of cirrus cloud fraction. Reference is 57-m spatial resolution Landsat data. All pixel sizes are diameter of the optical field of view. Each point represents cloud fraction for a single 58-km region over ocean.

effect of spatial averaging on relationships between cloud properties and optical properties in time- and space-averaged data.

3. Cloud height has the smallest horizontal spatial variability, followed by cloud particle phase/size. Finally, cloud visible optical depth has the largest spatial variability.

If all cloud properties are equally variable in space, then we must treat every cloud imager pixel as a unique cloud retrieval, totally independent of its neighbors. Neighboring pixels in this case do not impart any new information. At best they may be used in larger groups only to decrease the amount of instrument noise.

If, on the other hand, one or more of the cloud properties exhibits much larger spatial scales or less variability than the other cloud properties, then it is possible to group the data and derive additional information from collections of pixels that would not be feasible, or would be ambiguous, using a single pixel. Many cloud algorithms use exactly this assumption, but for different cloud properties. The spatial coherence algorithm (Coakley and Bretherton, 1982) relies on the uniformity of cloud height to derive estimates of overcast cloud layer properties, to separate these overcast pixels from broken cloud or variable emissivity pixels, and to ascribe an effective cloud amount to each variable pixel. Some recent studies of cloud particle size (Lin and Coakley, 1993) further assume that both cloud height and cloud particle size are constant over a distribution of pixels. The method of Arking and Childs (1985) assumed that cloud height and cloud visible optical depth were constant and adjusted cloud amount to achieve a consistent cloud retrieval.

Rigorous proof of these assumptions is not yet available, although for cloud height, the recent availability of ECLIPS (Experimental Cloud Lidar Pilot Study) lidar data for cloud base, and 3-mm radar data from FIRE (First ISCCP Regional Experiment) provide data sets adequate to begin a more thorough examination of this assumption. Uplooking LWP data such as taken during the FIRE experiments can be used to infer the variability of optical depth. We conducted an initial examination of this variability using the 1987 FIRE data from San Nicolas Island for LWP over a 19-day period, and cloud base altitude from ECLIPS lidar for a 5-day period. These initial data confirmed the usual qualitative assumption that cloud height is much less variable. These data sets are too limited to base global analysis on, however, and further work is needed in this area for a wider range of cloud types. The answer is likely to be a function of cloud type and whether cloud base or cloud top is most important. A very interesting data set in this regard is the global lidar data taken from the space shuttle in late 1994 by the Langley Lidar In-Space Technology Experiment (LITE). While LITE only obtained data for selected orbits during its 2 week mission it gave a tantalizing view of what will be available on future lidar and cloud radar satellite missions. Other critical future data sets will be long time series from 3-mm radar and lidar at ARM (Atmospheric Radiation Measurement) sites in the tropics, mid latitudes, and polar regions. The assumption used here that cloud particle size is more spatially contiguous than visible optical depth is based on aircraft reports that cloud liquid water content seems to vary more with cloud particle number than with cloud particle size. This assumption is also supported by initial analysis of satellite inferred cloud properties using the AVHRR visible channel (optical depth variability) and 3.7-μm channel (cloud particle size) as shown in Coakley et al. (1987) and Coakley and Davies (1986). A rigorous study of this conclusion over a large data set has not been carried out to our knowledge. Much of this data exists, at least for boundary layer clouds, convective clouds, and cirrus.

Given the importance of multilayer clouds to the LW surface radiation balance, and to the in-atmosphere radiative fluxes, the CERES algorithms will begin to address the issue of remote sensing of multilayer cloud systems. One of the key proposals for unscrambling complex cloud overlap cases is to allow cloud height information to propagate horizontally from single-layer to multilayer cloud observations. A key assumption is that the layers are reasonably independent, so that cloud heights in single-layer regions are similar to cloud heights in multilayer overlapped cloud regions. Clearly if the cloud layers are vertically close (1 km or less) they are likely to be strongly correlated. If they are vertically

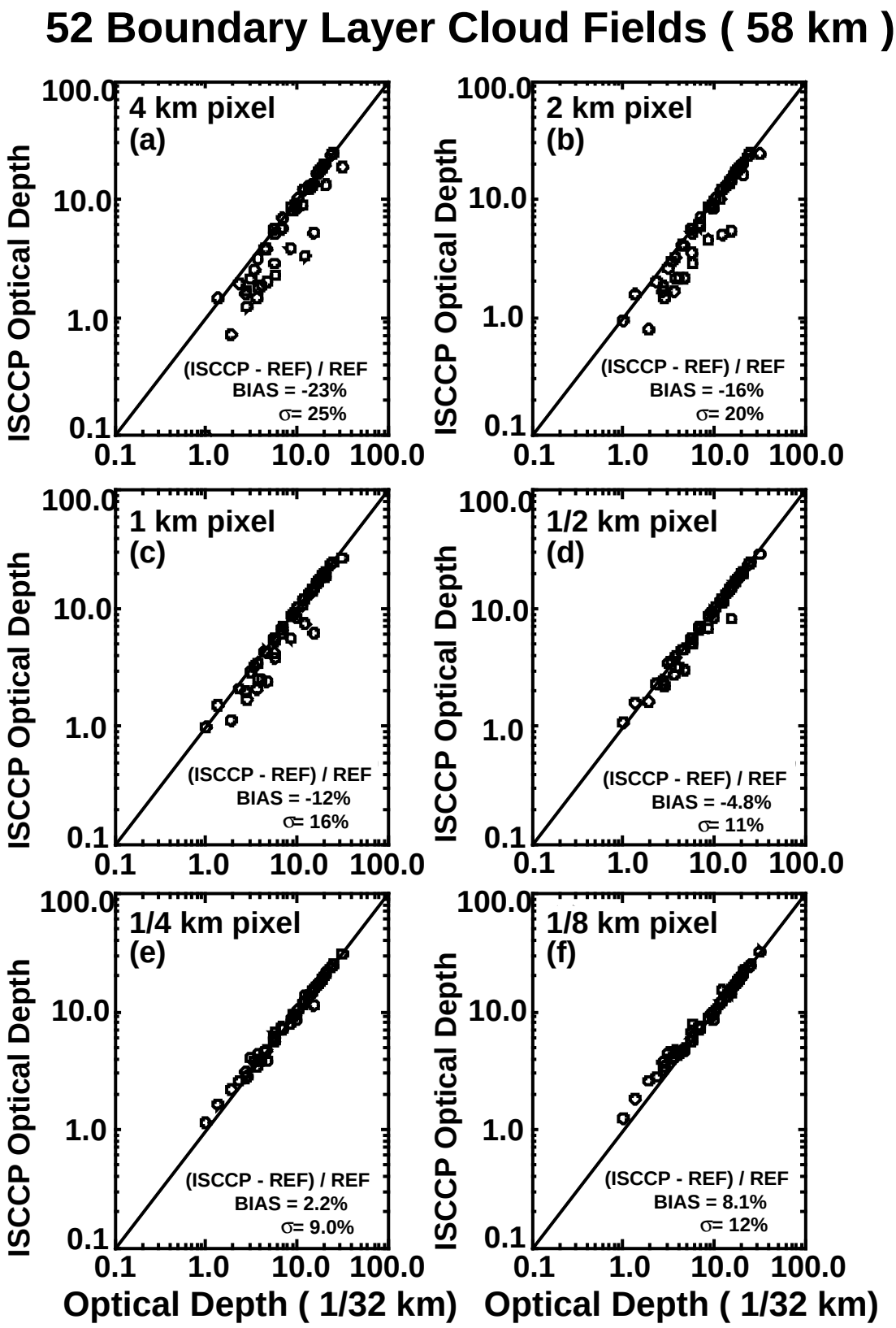

Figure 4.0-3. Effect of sensor spatial resolution on ISCCP-like estimate of cloud optical depth for boundary layer cloud cases. Reference is 57-m spatial resolution Landsat data. All pixel sizes are diameter of the optical field of view. Each point is a linear average of optical depth for cloudy pixels in a 58-km region.

separated by more than 6 km, they are probably poorly correlated (cirrus over boundary layer stratus). An exception to this would obviously be storm fronts, where large systematic cloud height changes occur over several hundred km.

Because of the difficulties encountered in remotely sensing multi-layer cloud systems, CERES will approach the remote sensing of multi-layer clouds in two distinct phases, as additional measurement capabilities become available.

The first phase starts with the launch of TRMM in 1997. The Release 2 CERES cloud mask algorithm will classify whether each CERES field of view is dominated by clear-sky, single level, or multi-level cloud (see Subsystem 4.1). Cloud physical properties, however, will be derived assuming each imager pixel within a CERES field of view contains only a single layer of cloud (Subsystem 4.3). During this first phase, selected data will be analyzed to combine the TRMM VIRS imager data with the TRMM Microwave Imager (TMI), and verify the feasibility of routine production of multi-layered cloud physical properties over ocean backgrounds. The microwave algorithms to determine simultaneous liquid water path (LWP) and cloud temperature have been developed (Lin et al., 1997a,b; Sheu et al., 1996) and initially tested using SSM/I data. Tests of the Lin et al. 1997 algorithm using theoretical simulations predicted a cloud temperature accuracy of between 3 and 6K (1σ) depending on the cloud LWP. Lower cloud temperature errors are found for larger LWP values. Initial data analysis has shown similar accuracy when intercomparing SSM/I microwave cloud temperatures and nearly simulataneous Meteosat thermal infrared imager cloud temperatures for single layer stratocumulus systems (Lin et al., 1997b). TRMM VIRS and TMI multi-layer cloud properties will be validated using the DOE ARM tropical site radar/lidar cloud height information and uplooking passive microwave LWP data to verify the performance of this multi-layer satellite technique for tropical cloud systems. If successful, it will be applied during the re-analysis of the TRMM data once new angular dependence models have been developed (subsystem 4.5). This technique can also be applied to EOS-PM data (MODIS plus AMSR) as well as EOS-AM (MODIS plus MIMR on METOP beginning in 2000). As for most passive microwave applications, the analysis is expected to be successful only over ocean backgrounds.

The second phase of multi-layer cloud analysis begins with the combination of MODIS infrared sounder (13 to 14 μm channels) data and window channel data to improve the treatment of optically thin high cloud over extensive low or middle level cloud. This technique (Baum et al., 1994) requires the use of infrared sounder channel data to provide the height and emissivity of the upper level thin cloud, and imager channel data to determine the properties of the lower level cloud. Unlike the passive microwave techniques, this method can be applied over both land and ocean backgrounds. Validation of this technique will be carried out primarily over the ARM tropical, midlatitude, and polar surface sites in the short term (1998 - 2000) and against satellite based cloud lidar/radar in the longer term. This technique can be applied to MODIS data, or to GOES-8 data. Unfortunately use of GOES-8 restricts validation to the Oklahoma ARM site and field experiments of opportunity such as LBA in tropical South America planned for 1999.

Note that the above two techniques will not handle the case of an optically thick water cloud overlying a lower water cloud layer. In this case, assumptions must be made about cloud overlap based on climatological analyses: random, maximum, or minimum overlap. Further discussions of this issue can be found in Hahn e al. (1982), Tian and Curry (1989), Wang and Rossow (1995). As a starting point in Release 2, CERES will assume that cloud layers are uncorrelated when separated in the vertical by more than 3 km. Finally, CERES assumes that no more than two cloud layers are present in each CERES field of view (see subsystem 4.4).

By 2000, it should be possible to evaluate the utility of the two multi-layer cloud algorithm strategies for use in the first major reprocessing of the CERES data using new angular models (2001 for TRMM, 2002 for EOS-AM). Note that the utility of the multi-layer cloud information is primarily for determination of the vertical distribution of longwave infrared fluxes, and will probably have little effect on the angular dependence models developed using only the Release 2 multi-layer cloud classifier. This is clearly true for the case of optically thick high cloud over any lower level cloud, but will have to be verified in the case of opti-

cally thin high cloud over boundary layer low cloud which may significantly affect the accuracy of the limb darkening models.

While encouraging initial progress has been made on observing multi-layer cloud systems in recent years (Baum et al. 1994; Lin et al. 1996a,b; Sheu et al. 1996; Wang and Rossow, 1995; Baum et al. 1995) a great deal of work remains. In support of this work, there is an urgent need for a spaceborne cloud lidar and radar system to achieve global accurate measurements of cloud overlap. Cloud lidar is optimal for low to moderate optical depth clouds and geometrically thin cloud layers, while cloud radar is optimal for moderate to large optical depth clouds and thick cloud layers.

4. Cloud layers separated by more than 3 km in height are independent.

The initial reason for this assumption is to allow the use of nearby single-layer cloud height observations to constrain the solution of optical properties for two-layer cloud overlap conditions. This assumption also enters into how to handle the time and space averaging of cloud overlap conditions. If the layers are independent, then cloud physical and optical properties can be saved in cloud height categories, where cloud properties for an imager pixel are categorized based on the effective cloud pressure, p_e

High Cloud:	$p_e < 300$ hPa
Upper Middle:	$300 < p_e < 500$ hPa
Lower Middle:	$500 < p_e < 700$ hPa
Low:	$700 < p_e < 1000$ hPa

p_e is the pressure in the atmospheric temperature profile which corresponds to the effective radiating temperature of the cloud. For a thin cloud this is the cloud center; for a thick cloud it is the cloud top. This can be thought of as the radiative center of mass for the cloud as viewed from the TOA in the thermal infrared part of the spectrum. Given the independence of cloud layers, we do not require that separate cloud properties be saved for every overlap combination of two cloud height categories. Instead, we simply save the fraction of space or time covered by each of the 11 cloud overlap conditions:

1. No cloud
2. Low cloud only
3. Lower middle cloud only
4. Upper middle cloud only
5. High cloud only
6. High cloud over upper middle cloud
7. High cloud over lower middle cloud
8. High cloud over low cloud
9. Upper middle cloud over lower middle cloud
10. Upper middle cloud over low cloud
11. Lower middle cloud over low cloud.

The selection of category pressure boundaries is somewhat arbitrary. The current selection is based on the following criteria:

- A minimum of three cloud layers to distinguish major cloud types: high/middle/low clouds
- A pressure boundary at 500 hPa, the level chosen for CERES initial atmospheric radiative flux analysis, thereby separating the troposphere into two parts for radiative heating
- Pressure boundaries which are a subset of those used by ISCCP, so that direct comparisons can be made to the ISCCP data; ISCCP has boundaries which include 680 and 310 hPa
- Maintain a minimum of about 3-km separation between height categories, so that layers are often independent

These criteria led to the selection of four cloud height categories and boundaries at 700, 500, and 300 hPa. In the tropics, the 300-hPa boundary occurs at a temperature of about 240K, similar to the 235K threshold often used to distinguish precipitating clouds. This selection should prove useful when comparing radiative and latent heating profiles estimated using TRMM data.

A schematic diagram summarizing the cloud height categories and layering assumptions is shown in Figure 4.0-4 which is taken from Subsystem 4.4.

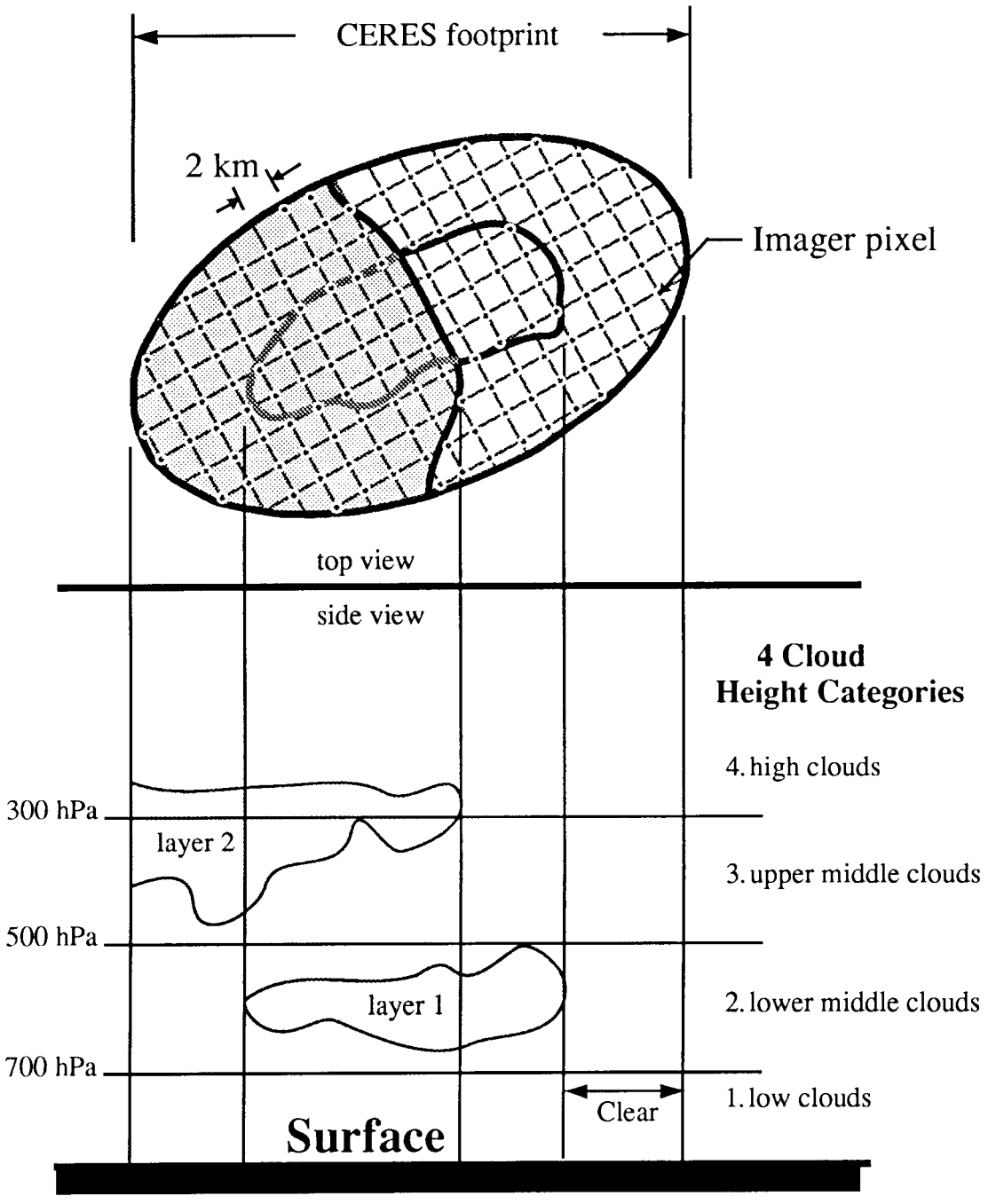

Figure 4.0-4. Schematic diagram of vertical and horizontal cross sections of imager pixel cloud properties matched to CERES field of view. 2-km imager pixel spacing is typical of VIRS on TRMM. Data tables can be found in Subsystem 4.4.

5. Clouds are sufficiently varied in time and space that there is currently no single cloud algorithm that works well for all cloud types and cloud properties.

As is often the case when attacking a formidable problem, each cloud algorithm has commonly examined a small piece of the whole cloud retrieval problem. ISCCP has developed the most complete analysis to date, although the ISCCP algorithm is severely limited by the restriction to use only two spectral bands, a visible and an infrared window channel. The CERES cloud analysis will have a more complete set of measurements to use, including all five of the AVHRR channels, the 1.6-μm channel on VIRS and MODIS, new channels on MODIS, as well as passive microwave data. In spite of this additional information, there is still no single algorithm available to handle the wide diversity of cloud properties observed over the globe. Instead, a robust cloud analysis which gains the best information from each spectral channel and instrument will by nature be forced to combine multiple cloud algorithms.

Clear and accurate combination of diverse algorithms is a difficult task. In order to achieve this strategy, CERES has a team which includes experts in many of these different approaches. This document describes the current understanding of the best way to implement such a combined algorithm. Like ISCCP, the cloud algorithm is divided into a cloud detection and a cloud optical property stage. Unlike ISCCP, the algorithm also includes an additional stage for the determination of well-defined cloud layers.

The discussion in Section 4.0.4 summarizes the current strategy for selection and/or merging of cloud retrieval algorithms for CERES cloud property retrievals (mask, height, and optical properties). Because of the substantial differences in capability between MODIS and VIRS, the VIRS algorithms will be discussed in 4.0.4.1. Section 4.0.4.2 discusses how the additional MODIS capability is integrated into the algorithms and effects algorithm selection.

6. Accurate relationships between cloud and radiative fluxes require accurate spatial and time matching of both imager-derived cloud properties and CERES broadband radiation data.

There are three primary reasons to closely link the instantaneous CERES radiances to cloud imager derived cloud properties.

First, the development of anisotropic models from CERES rotating azimuth plane scanner data requires that CERES broadband radiances be accurately classified as a function of cloud and surface properties. A particularly critical cloud property for SW and LW anisotropy is cloud optical depth. Tests were made using FIRE stratocumulus uplooking passive microwave observations of LWP (e.g., Cahalan et al. 1994) taken every minute for 19 days in July 1987 at San Nicolas Island. At a mean wind speed over the period of 5 m/s, the 1-minute sampling corresponds to a cloud advection of about 300 m. A running time average was then applied to the data to simulate the 20-km CERES footprint scale (roughly a 60-minute running average). Finally, the time-averaged CERES footprint data were time lagged to simulate the effect of a spatial (or temporal) mismatch in the cloud imager data (providing LWP or cloud optical depth) and the broadband radiation data. If the lagged rms difference in LWP is required to be 5% or less, then the 20-km average can be mismatched by no more than 1 km (or about 3 minutes). The rms LWP error was roughly linear in the lag time or distance. We conclude that accurate angular models are likely to require close matching of cloud and radiation data. Further tests will be conducted using Landsat data to extend these 1-D results to two dimensions.

Second, if TOA flux measurements are to be used to constrain the radiative fluxes calculated using cloud imager derived cloud properties, then a close match of these properties must be obtained. Because cloud physical and optical properties are nonlinearly related to radiative fluxes, rms errors in matching cloud and radiation data should be kept to less than 10% to avoid bias errors. Tests of this sensitivity will be conducted using simulations similar to those above, but including radiative flux calculations on high resolution cloud imager properties such as AVHRR Local Area Coverage data.

Third, the complexity of relationships between cloud properties and radiative properties increases as clouds become multilayered. Tian and Curry (1989) found that while single-layer clouds dominated observations at a 45-km scale (similar to a single CERES footprint), multiple-layer clouds dominated at 220 km (similar to an ERBE grid box). This suggests that for some studies, there is an advantage to close ties of cloud properties and radiative fluxes at not only the scale of large grid boxes, but also at the scale of individual CERES footprints.

The CERES strategy is to represent the distribution of energy received at the CERES broadband detectors by the point spread function (Subsystem 4.4). The point spread function includes the effects of detector response, optical field of view, and electronic filters (Subsystem 1). Cloud imager derived cloud properties will be convolved with the CERES point spread function to derive properties appropriately weighted and matched to the CERES fields of view. Note that the nominal 2σ accuracy of the navigation for the EOS and TRMM platforms is less than 1 km, sufficient to allow an accurate mapping of imager pixel data into CERES fields of view.

7. Anisotropy of cloud and surface scenes can be determined by compositing a large ensemble of scenes where each scene is viewed at one instant of time from only 1 or 2 directions.

The rapid variability of clouds in space and time places a fundamental limitation on measuring radiative flux from space. There are no sufficiently homogeneous targets for which a satellite can view all 2π steradians of a “target” at the same time. The flat plate or active cavity instruments which view 2π steradians from satellite altitude respond to about a 2000-km region on the Earth, guaranteeing inhomogeneity. Therefore, all measurements of flux from space require compositing over time. The scanning radiometers such as the Nimbus-7 ERB or ERBE scanners select a small angular field of view in order to measure individual scene types (forest, cumulus, stratus, cirrus, etc.). This requires the conversion of the radiance measured in a single direction to the desired radiative flux. In order to improve spatial sampling over the globe, scanning radiometers usually scan in a cross-track pattern, limiting angle views to a small systematic subset of the full angular space.

For SW radiation, anisotropy is a function of viewing zenith angle, viewing azimuth angle, and solar zenith angle (Suttles et al. 1988; Wielicki and Green, 1989). Typical scanning instruments measure only a small portion of this 3-D angular space. The Nimbus-7 ERB instrument was designed to sacrifice spatial sampling to obtain improved angular sampling over the entire 2π hemisphere (Taylor and Stowe, 1984). ERBE used these observations to develop the 12 ERBE angular distribution models (ADM’s) as a function of cloud fraction and surface type (ocean, land, desert, snow/ice) (Suttles et al. 1988).

Unfortunately, the ERBE models are unsatisfactory for CERES for three reasons. First, postflight analysis (Suttles et al. 1992) has shown that the estimated SW albedo systematically increases with viewing zenith angle and the estimated LW flux decreases with viewing zenith angle. The ERBE models based on Nimbus-7 observations underestimate the amount of anisotropy. Second, the albedo bias is a function of solar zenith angle, and therefore a function of latitude (Suttles et al. 1992), which will affect the inference of equator-to-pole heat transport. Third, the models only depend on cloud amount, so that the rms error in deriving instantaneous fluxes is estimated as roughly 12%. This instantaneous noise is primarily caused by the inability of ERBE and Nimbus 7 to measure cloud optical depth, the largest source of varying anisotropy (Wielicki et al., 1996).

Tests of the ADM bias have examined three possible causes: incorrect scene identification by the ERBE maximum likelihood estimation technique (Suttles et, al. 1992; Ye, 1993), incorrect assumptions in building the ERBE ADM’s, and the dependence of ADM’s on spatial scale (Ye, 1993; Payette, 1989). CERES will fly a scanner which will rotate in azimuth angle as it scans in elevation, allowing the development of a new set of ADM’s. All three candidate problems are being examined with current data in preparation for designing the CERES ADM’s.

First, scene identification will be greatly improved by matching VIRS- and MODIS-derived cloud properties to each CERES field of view. This will provide the basic cloud typing for development of new ADM's. ADM's will be derived as a function of cloud amount, cloud optical depth/emittance, cloud height, particle phase, and cloud particle size. Second, one of the critical assumptions of the Nimbus-7 and ERBE ADM's was that cloud anisotropy and cloud albedo are uncorrelated. For the case of increasing cloud optical depth, this is clearly a questionable assumption. This assumption will be removed for CERES by using the radiance pair method discussed in Subsystem 4.5. This method uses the rotating azimuth plane CERES scanner to obtain views of the same target at nearly the same time from two different viewing angles. The pairs are used to obtain reflectance ratios which eliminate the dependence on target albedo. Finally, studies will examine the dependence of field of view spatial scale in testing of new CERES ADM's.

4.0.4. Algorithm Outline

Because cloud fields are highly variable in space and time, the process of both cloud detection and cloud property determination from space can become very complex. This is true especially over variable backgrounds such as mountains, desert, or snow and ice. As a result, no single cloud algorithm works well for all cloud types over all backgrounds. In order to deal with this complexity, the CERES cloud algorithm has broken this task into three relatively independent functions:

Subsystem 4.1—Clear-sky determination and cloud detection.

Subsystem 4.2—Cloud height determination.

Subsystem 4.3—Cloud optical property retrieval.

Following the cloud retrieval over a swath of cloud imager data, three final steps are carried out to obtain TOA and surface radiative fluxes for each CERES broadband measurement.

Subsystem 4.4—Convolution of imager cloud properties with CERES footprint point spread function.

Subsystem 4.5—CERES inversion to instantaneous TOA fluxes.

Subsystem 4.6—Empirical estimates of shortwave and longwave surface radiation budget involving CERES measurements.

The final result is a set of cloud properties and radiative fluxes for each CERES footprint. The final cloud properties are grouped into four cloud height categories with height boundaries at pressures of 700, 500, and 300 hPa. Since more than one cloud layer is allowed in a CERES footprint, we also save the fraction of the footprint covered by cloud imager pixels which showed evidence of overlap of any two of the four cloud height categories. Only two of the four cloud height categories are allowed to overlap in a single cloud imager pixel. For Release 2, we assume that the four cloud height categories are independent, so that cloud properties in any given height category are independent of whether or not they were overlapped with any other height category. This simplification allows us to keep cloud properties for only four categories, as opposed to all possible combinations of cloud height categories. Cloud overlap is only saved as the fractional area of overlap between all combinations of two of the four cloud height categories. CERES saves not only the frequency of occurrence, but also the average and standard deviation of all cloud properties separately for each cloud height category. In this case, even very small cloud height shifts can be detected within each cloud height category.

All cloud properties are weighted with the CERES point spread function so that CERES-measured broadband TOA fluxes can be used to directly constrain radiative calculations of surface and in-atmosphere fluxes produced using the cloud imager cloud properties. These CERES footprint averages represent a very specific view or composite of cloud physical and optical properties designed to facilitate studies of the role of clouds in the Earth's radiation budget. A table of the CERES cloud products for each CERES footprint can be found in Subsystem 4.4.

Finally, where possible, direct parameterizations of TOA radiative fluxes to surface radiative fluxes are derived. These surface flux estimates for each CERES footprint are saved in the SSF output product of Subsystem 4, as well as in spatially gridded and time-averaged forms in the SURFACE products (Subsystems 9 and 10). Direct parameterization of TOA to surface fluxes is used as an alternative approach to the calculation of surface radiative fluxes using cloud properties and radiative models used in the ATMOSPHERE data products (Subsystems 5, 6, 7, and 8).

A full description of the Subsystem 4 input and output products can be found in appendixes A and B.

4.0.4.1. TRMM VIRS 5-channel Data

4.0.4.1.1. Cloud Mask

In pre-launch studies we have examined the performance of both multi-spectral threshold algorithms similar to SERCAA, paired histogram texture algorithms, and fuzzy logic algorithms. To date, these studies have indicated similar or better performance of the multi-spectral threshold algorithms, which will be used as the baseline for the TRMM at-launch cloud mask algorithm. If validation studies comparing cloud mask results against surface observers (many sites, but subjective validation data) and surface lidar/radar (few sites, <10, but objective data) then the texture and fuzzy logic methods may be reconsidered. In general the artificial intelligence methods are more computationally intensive, and if necessary, their use may be restricted to especially difficult targets such as mountains and snow/ice backgrounds. At present, the multi-spectral threshold cloud mask algorithm also includes detection of multi-layered versus single-layered cloud within the CERES field of view.

4.0.4.1.2. Cloud Height / Radiative Temperature / Thickness

There are two basic methods available for cloud height/temperature determination using the TRMM VIRS 5-channel instrument.

a) Multi-spectral imager

- daytime: 0.65, 3.7, 11, 12 μm

  (similar to ISCCP with added microphysics determination)

- night-time 3.7, 11, 12μm

  (new extension to improve non-black cloud heights at night)

b) Spatial Coherence

- day/night independent: 11μm

  (uses locally uniform radiance to detect optically thick layers.

During daytime conditions, the optically thick layers identified by the spatial coherence technique will also be found straightforwardly by the multi-spectral technique. The multi-spectral technique has the advantage of correcting cloud heights for non-black cloud, and as a result is expected to be the most accurate cloud height algorithm during the day. At night, however, there is an ability for the Spatial Coherence method to provide independent information on cloud layering that can be used as input to the multi-spectral algorithm. This will be the strategy used at TRMM launch. Pre-launch tests of the multi-spectral nighttime algorithm on single layered optically thin cloud over the ARM Oklahoma site (using similar spectral channels from GOES) show encouraging results. Multi-layer cases remain problematic. To date, all cloud thickness algorithms are based on an approximate empirical relationships between cloud optical depth and cloud physical thickness, where different relationships are used for water and ice clouds based on FIRE field experiment results (see subystem 4.3).

4.0.4.1.3. Cloud Optical Properties (τ(0.65 μm), ε(11 μm), particle phase/size)

There are two basic approaches to derivation of cloud optical properties using the TRMM VIRS 5-channel instrument:

a) Use of 3.7 μm for primary microphysics information:

- daytime: 0.65, 3.7, 11, 12 μm: 0.65 μm optical depths 1 to 50
- nighttime: 3.7, 11, 12 μm: 0.65 μm optical depths 1 to 6

  (solved simultaneous with cloud height/temperature)

b) Use of 1.6 μm and 3.7 μm for primary microphysics information

- daytime: 0.65, 1.6, 2.1 μm: 0.65 μm optical depths 1 to 50
- nighttime: NOT APPLICABLE

At present, CERES will use option a) as the baseline. After launch we will examine the utility of adding the 1.6 μm channel. This channel may prove most useful in cases of very large ice crystals, with equivalent diameters of 100 μm or greater.

4.0.4.2. EOS-AM and EOS-PM MODIS Data

4.0.4.2.1. Cloud Mask

The basic algorithm methodology is not expected to change from a multi-spectral threshold analysis for MODIS. MODIS does, however, add higher spatial resolution and several spectral channels which will be useful in adding to the ability to distinguish clouds:

-1 .38 μm daytime detection of thin cirrus over low cloud or land/ocean

- higher spatial resolution (0.25 km at 0.65 μm, and 1.0 km all others)

4.0.4.2.2. Cloud Height / Radiative Temperature / Thickness

A third major methodology for cloud height is added for MODIS: CO_2 slicing using the 13.3, 13.6, 13.9 and 14.2 μm channels. This methodology works equally well for day or night conditions, and can determine imager pixel level effective cloud amount (emittance times cloud fraction) as well as the cloud height. The CO_2 slicing methodology has some advantages over the multi-spectral imager approach:

- independent of day/night
- less dependence on particle size
- no dependence on the scattering phase function of ice crystals
- for thin cirrus, the retrieval is only weakly affected by underlying low cloud. In contrast , during daytime, the presence of a low stratus layer will defeat the ability of an ISCCP-like multi-spectral cloud height algorithm to detect thin cirrus, because the visible optical depth is controlled by the lower stratus layer.

The major disadvantage of the CO_2 slicing method is the methods relatively poor performance for low clouds (as a result of low thermal contrast with the surface). These relative strengths and weaknesses suggest a combination of algorithms that uses the CO_2 slicing method for middle level and high clouds, and the multi-spectral techniques for low clouds. The initial strategy for use at launch of MODIS on EOS-AM in June 1998 will be to use the CO_2 slicing technique only when the cloud signal

(measured radiance - clear radiance) is relatively large in the 13.6 μm channel with a weighting function peak at 700 hPa. This will indicate the presence of a middle or high level cloud, and will assure reasonable accuracy in the methodology. The value of the 13.6 μm cloud signal used for the algorithm transition between multi-spectral and CO_2 slicing will be determined using validation data from the ARM sites lidar and radar cloud height measurements. It is also expected that the CO_2 slicing method, when combined with the multi-spectral imager algorithm will allow more accurate retrievals of multi-layered cloud, at least for the case of optically thin cloud (e.g. cirrus) over lower optically thick cloud (Baum et al. 1994, 1995)

4.0.4.2.3. Cloud Optical Properties (τ(0.65 μm), ε(11 μm), particle phase/size)

For 0.65 μm cloud optical depth, MODIS improves the accuracy by providing 0.25 km spatial resolution in the 0.65 μm channel. This minimizes errors due to cloud inhomogeneity and due to pixel beam filling assumptions (See Fig 4.0-3). The algorithm, however, is basically unchanged from TRMM. For cloud emissivity, the CO_2 slicing method at night should allow improvement in cloud emissivity estimation by virtue of its more accurate determination of the radiating temperature of optically thin cloud (see previous section on MODIS enhancements of cloud height determination). For microphysics, there are two spectral channels which potentially improve the cloud microphysics capabilities of MODIS over those of VIRS:

- 8.5 μm: used together with 3.7/11/12 μm at night to allow retrieval of larger particle sizes (De > 100 μm).

- 2.1 μm: used together with 0.65/1.6 μm during the day only to derive cloud particle size and phase. Because ice cloud scattering phase functions are still an area of uncertainty, the optimal daytime retrieval strategy would strive for consistency in all channels with microphysics information: 0.65 / 1.65 / 2.1 / 3.7 / 8.5 μm. Such a strategy is currently beyond the capability of any existing algorithms, but may be possible in the first few years after EOS-AM launch.

CERES will focus initially on adding the 8.5 μm channel at night, since this retrieval is much less certain than that during the day.

4.0.4.3 Cloud Validation Data and Post-launch Algorithms

In all cases of cloud algorithm decisions, the postlaunch comparisons against long-term surface sites (ARM plus a few additional BSRN sites) will be used to decide on the optimal algorithm approach and under what conditions it is applied. These comparisons will focus on multiple climatic regions and seasons, with intercomparisons of satellite and surface based cloud data at every satellite overpass. This long-term focus is necessary to test the algorithms with robust statistical significance over a wide range of:

- cloud conditions

- surface conditions

- solar illumination

- satellite viewing angle (zenith and solar azimuth)

The ultimate cloud algorithm for MODIS and VIRS data is one which derives cloud properties which satisfy the complete observed spectral wavelength dependence and spatial dependence for the VIRS and MODIS channels. The use of multiple spatial and spectral algorithms by CERES is a step in this direction.

4.0.5. Algorithm Releases

The CERES algorithm will be designed in three major "releases". Release 1 was delivered to the Langley DAAC in February 1996, and was the first release capable of processing global satellite data. The release 1 algorithm was designed to use existing AVHRR global satellite data for October 1986 and to focus on daytime retreival of cloud amount, height, thickness, optical depth, particle size and particle phase. The Release 1 algorithm was used to:

- Design a framework to integrate multiple cloud retrieval algorithms
- Discover problems in exception handling: how to process imperfect data.
- Begin development and testing of QC reports.
- Estimate realistic processing loads for future production processing.
- Discover gross algorithm problems by examination of global results.
- Automate research algorithms.

A successful framework was developed, exception handling was integrated, and realistic processing loads estimated using 16 days of global AVHRR/ERBE data (see section 4.0.7 for details). Examination of daily global maps of derived AVHRR cloud particle size demonstrated an ambiguity (multiple solutions) in cloud particle size retrieval in the backscattering part of the AVHRR scan. The Release 1 cloud algorithm included the following characteristics:

- 20 km resolution ecosystem type, elevation and water/land map
- Explicit treatment of the anisotropy of clear sky land and ocean reflectance
- Multi-spectral global cloud mask
- Cloud optical depth derived similar to ISCCP, but incorporating the ice crystal scattering phase functions from Takano and Liou (1989) for ice clouds
- Optically thin cloud heights adjusted as in daytime ISCCP algorithm
- Cloud particle size and phase (water/ice) derived using 0.6/3.7/11μm channels

The release 2 cloud algorithm is now in development, and is scheduled for delivery to the Langley DAAC in July, 1997. This algorithm is designed for use with the VIRS instrument on TRMM. Release 2 will concentrate on several improvements to the Release 1 algorithms:

- Addition of daytime multispectral cloud mask over snow/ice
- Addition of daytime multi-layer cloud mask
- Update capability for clear-sky background map, especially for changes in surface temperature, but also for seasonal vegetation change
- Addition of 3.7 and 11 μm surface emissivity maps
- Addition of NOAA oceanic aerosol retrieval algorithm
- Particle size retrieval using 0.6/3.7/11/12 μm to minimize ambiguity in the backscatter observations.
- Addition of nightime 3.7/11/12 μm retrieval of emissivity and particle size/phase.
- Addition of spatial coherence algorithm for assistance with cloud layering, especially at night
- Addition of routine automated QC reports

- further development of both regional and global data visualization tools
- ability to process GOES-8 imager data

Elements of the Release 2 algorithm are being validated against past FIRE experiment data, as well as the ARM Oklahoma CART site data set.

Release 3 will be designed for use with the MODIS data on EOS-AM (launch in June 1998) and EOS-PM (launch late 2000). This release will incorporate the additional cloud spectral channels on MODIS (1.38, 2.1, 8.5, 13 - 14 μm). It will also include improvements for the reprocessing of the TRMM data as well. Timing of the TRMM reprocessing depends on development of the new angular dependence models using the VIRS and CERES rotating azimuth plane data (approximately 24-30 months after TRMM launch). Expected Release 3 algorithm improvements include:

- addition of infrared sounder cloud height/emissivity retrieval method
- addition of night-time cloud mask over snow and ice backgrounds
- potential addition of smoke mask for biomass burning
- potential addition of multi-layer cloud retrieval using infrared sounder and imager channels (thin high cloud over extensive low thick cloud).
- potental addition of multi-layer cloud retrieval using passive microwave and imager channels (thick high cloud over extensive low cloud).

Decisions on addition of the multi-layer algorithms will depend on off-line analysis and validation of these algorithms using combined VIRS/TMI data on TRMM, AVHRR/HIRS on the NOAA satellites, and the GOES-8 imager. These are the most challenging aspects of cloud retrieval, and will require significant advances, although initial results are encouraging (e.g. Baum et al., 1994; Lin et al., 1997a,b). Note that passive microwave imagers of the type used to determine water cloud altitude in Lin et al. 1997a,b will be on the TRMM and EOS-PM platforms, and will be available in a sun-synchronous orbit similar to EOS-AM on the European METOP platform starting in 2000. Initial validation of these multi-layer approaches will concentrate on field experiments and the 3 DOE ARM sites. In the longer term, a satellite cloud radar and lidar mission would be required for global validation. Such active cloud sensing satellite missions are being proposed as part of the new EOS ESSP program, but are not assured at this time.

4.0.6. Validation

The CERES Validation Plans are currently being developed. Following a peer review in late 1996, the Validation Plans will be made available on the WWW in August of 1997. In the interim, a separate document containing the Validation Plan Summary Charts for each major subsystem has been developed to accompany these ATBD's.

4.0.7 Cloud Retrieval (Susbystems 4.1, 4.2, and 4.3) Data Processing Scheme

4.0.7.1 Objectives

The Cloud Retrieval Subsystem's objective is to use high spectral and spatial resolution cloud imager data to determine cloud microphysical and optical properties. This provides a set of pixel cloud properties that are mapped onto the CERES footprint in the next process, documented in Software Design Document (SDD) 4.4. The major Cloud Retrieval science requirements are illustrated in Figure 4.0-5 and include:

1. Prepare a "chunk" of pixels (multiple scan lines of imager data): attach the imager radiances and various ancillary data to each imager pixel within the chunk. Classify each pixel as clear, cloudy,

or uncertain. The pixel classification process uses various tests on the imager radiometric data and ancillary data to determine a cloud mask.

2. Determine cloud macrophysical properties (cloud layer and cloud top pressure) for cloudy pixels (ATBD 4.2).

3. Determine cloud microphysical and optical properties (base and effective radiating center temperature and pressure, phase, particle size, optical depth at 0.65 micron, water/ice path, emittance at 10.8 micron) for cloudy pixels (ATBD 4.3).

The primary input data sets for the Cloud Retrieval Subsystem are:

1. The Cloud Imager Data (CID) data product contains time code, pixel location, viewing geometry, and radiance data. For the TRMM mission, CERES will use the Visible Infrared Scanner (VIRS) cloud imager data. For the next launches on EOS AM and PM spacecraft, CERES will use selected channels from the Moderate Resolution Imaging Spectrometer (MODIS) imager data. The Release 2 test data are Advanced Very High Resolution Radiometer (AVHRR) imager data from the NOAA-9 spacecraft.

2. A set of ancillary surface maps provide elevation, water content, snow, ice, ecosystem, and a condensed ecosystem/terrain map on a 10-minute equal-angle grid. Higher spatial resolution ancillary maps will be incorporated as they become available.

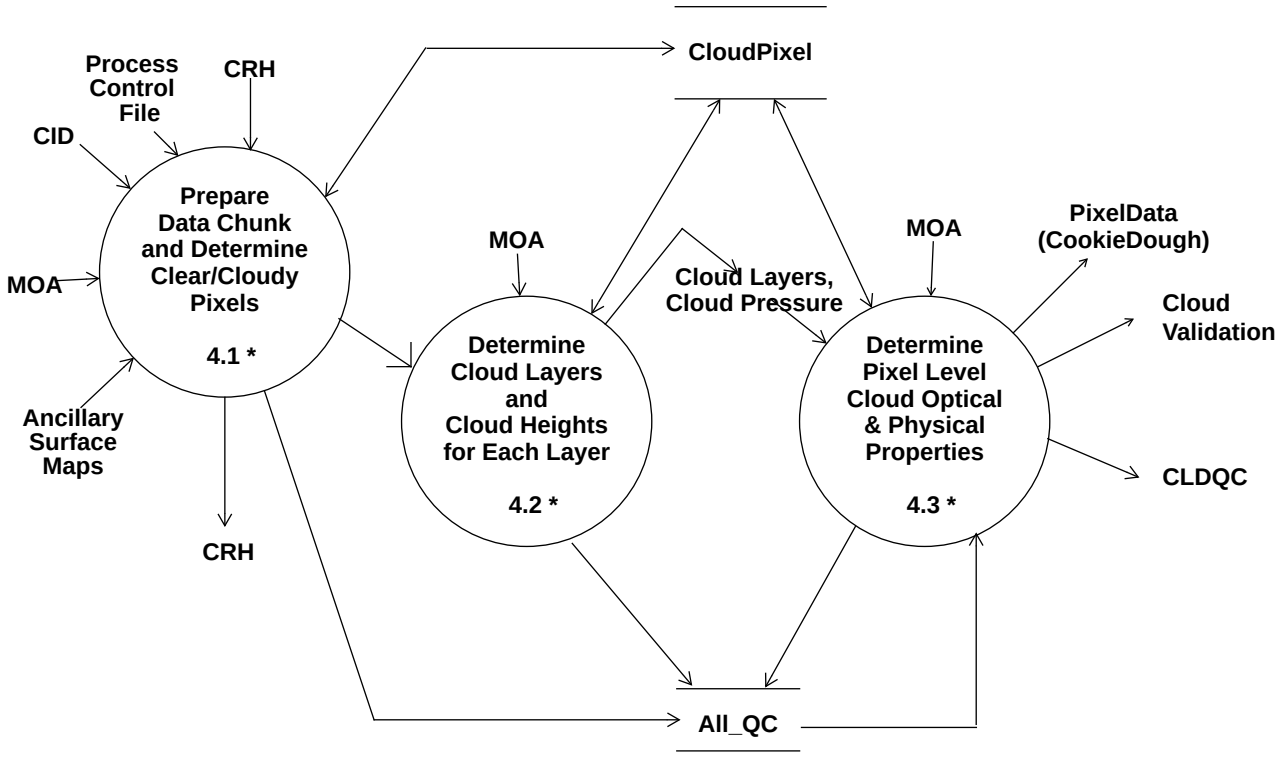

Figure 4.0-5. Subsystem 4.1 - 4.3 High-level Data Flow Diagram

3. The Meteorological, Ozone, and Aerosol (MOA) data product contains meteorological data (surface temperature and surface pressure; 58 atmospheric levels of temperature, humidity, and ozone; 18 levels of wind; precipitable water, and total column ozone, and aerosol optical depth on the CERES defined grid. (see CERES Subsystem 12).

4. The Clear Radiance History (CRH) data product contains the mean albedo, mean brightness temperature, and the cosine of the solar zenith angle on a 10-minute equal-angle grid. Standard deviations of albedo and brightness temperature are also kept.

The data sets which are input to science algorithms are acquired and/or developed by the Cloud Working Group. A Process Control File (PCF) specifying file names and run-time parameters is prepared by the Distributed Active Archive Center (DAAC) personnel. PCFs are prepared by the development team during development for testing purposes and are part of the DAAC delivery package.

The output products are the pixel-based cloud properties needed by the convolution process (Table 4.4 in ATBD 4.4), a validation product, Status Message Facility (SMF) log files, and Quality Control (QC) reports. The hourly output products are described in greater detail in the Data Products Catalog.

4.0.7.2 Key Concepts

This section discusses the major concepts behind the design of the Cloud Retrieval Subsystem.

- *Imager pixel*
- *Data chunk*
- *Bounding rectangle*
- *Master pixel*
- *Chunk loop*
- *Algorithm loop*
- *The framework*
- *Quality edit checks*

Imager pixel refers to a single cloud imager field-of-view, which ranges from 0.25 - 1 km for MODIS pixels, 2 km for VIRS pixels, and 4 km for AVHRR-GAC (Global Area Coverage) pixels. Some of the algorithms process one pixel at a time and some of the algorithms process arrays of pixels at a time.
Data chunk: The Cloud Retrieval Subsystem processes a chunk of imager data at a time. A chunk is a selected number of imager scanlines, which must be at least as large as the largest array of data any science algorithm needs.
Bounding rectangle: After reading the imager data chunk, the diagonal corner latitudes and longitudes of a rectangle that circumscribes the imager chunk are computed. These "bounding" latitude and longitude pairs are used to input a corresponding set of grids from the various input surface characteristic maps, the gridded MOA data set, and the gridded CRH data set. These data form part of a set of attributes that are associated with each imager pixel; each pixel is known as ’master’.
Master pixel: The framework prepares the master pixel by attaching parameters from input data, from calculated parameters, and from science algorithm results. The master pixel serves as a resource from which to select only the attributes a particular science algorithm requires. The master pixel consists of imager radiances and reflectances, the surface characteristics, the geotype, solar angles, clear-sky historical data, various flags, pointers to a set of 3-dimensional meteorological profiles, and algorithm results.
Chunk loop: The Cloud Retrieval Subsystem processes one chunk of imager data at a time. The chunk loop continues until there are insufficient data in the imager input hourly file to form the last chunk. The leftover scanlines will be processed with additional scanlines from the next hourly input file in Release 2.

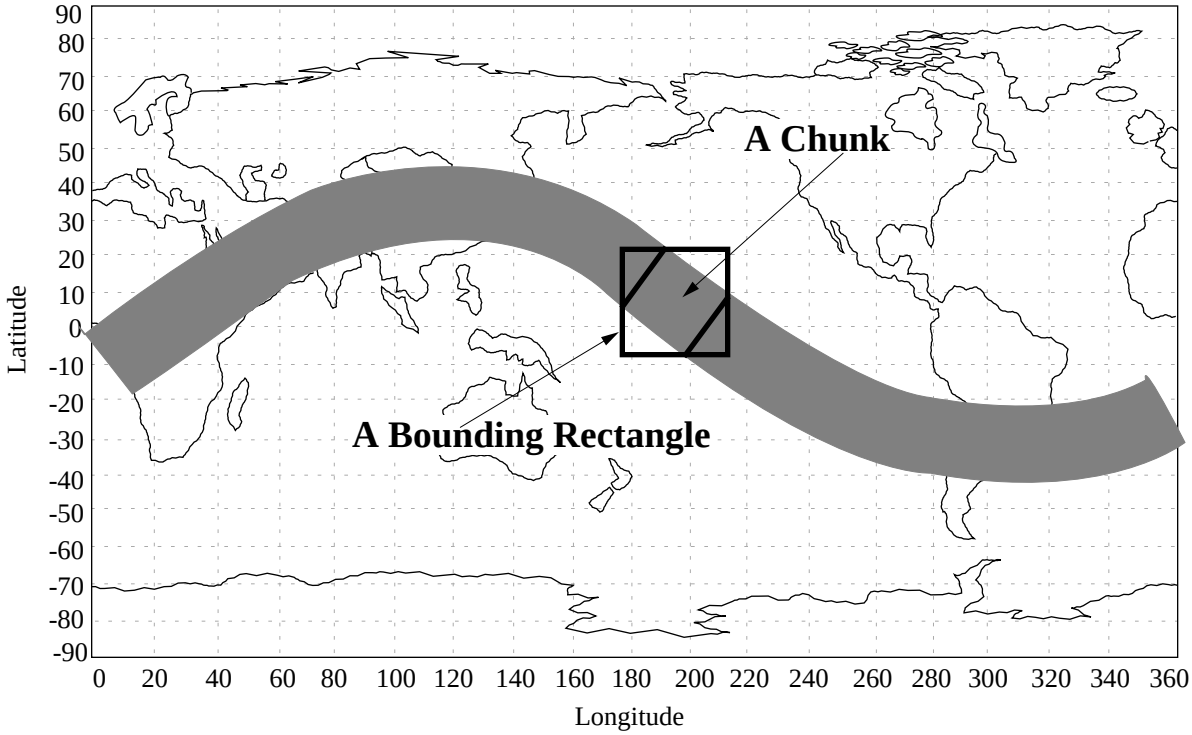

Figure 4.0-6 shows an arbitrary satellite orbit swath with an illustration of a data chunk and the bounding rectangle.

Algorithm loop: Surrounding each science algorithm is an input interface routine that does the tailoring from the master pixel for the algorithm. On the output side of each algorithm is another interface routine that receives the algorithm results and attaches it to the master pixel. If a particular algorithm has been selected to execute, an interface is prepared, an algorithm is executed, and results are stored. The code loops through all of the science algorithms that are selected for a particular run.

The framework interfaces with the input data, the algorithms, and the output data. The framework accesses and prepares input data for each science algorithm, executes the algorithm, and collects the results. The framework initializes the output files and writes results as processing proceeds. The framework provides the flexibility to add, replace, or delete a particular contributed science algorithm and to selectively execute it.

Quality edit checks for bad input data are made and fill data are used if the input data within an imager scanline are unusable. No fill scanlines are provided when entire scanlines are missing. Limit checks to ensure that the input data are within reasonable limits are implemented. Data that are outside these limits are excluded from further processing, and a diagnostic message is generated. Quality checks on science results and within the algorithm, along with science algorithm error-handling, will be evolving throughout Release 2.

4.0.7.3 Architectural Design

This section discusses two high-level views of the Cloud Retrieval Subsystem. The dynamic view is shown in the flowchart in Figure 4.0-7. The design approach provides a framework that serves data to the algorithms and manages algorithm results. Processing proceeds through two major loops. The

outer chunk loop processes pixels in scanlines in a chunk until all chunks in the hour imager data are processed. For each chunk, the three steps in the algorithm loop are processed for each algorithm that has been selected for the particular job.

The major steps and logic are

1. Initialize the cloud process, get the filenames, open the input files, check all input file header records, and open the output files.

   Steps 2 through 6 are the outer chunk loop. Process all chunks within the hour.

2. Prepare a "chunk" (multiple scan lines of CID imager data) of master pixels: Attach the imager radiances and reflectances, location data, various ancillary input surface conditions, clear-sky history information, and pointers to the meteorological profiles to each pixel within the chunk.

   Steps 3 through 5 are the inner algorithm loop: For each algorithm selected:

3. Prepare tailored data structures for the algorithm by extracting the required parameters from the master pixel.

4. Invoke a science algorithm chosen from the following major catagories

   a) Classify each pixel as clear, cloudy, or uncertain. The pixel classification process uses various tests on the imager radiometric data and ancillary data to determine a cloud mask (ATBD 4.1). The Release 2 algorithms include the CERES set of cloud mask threshold tests for determining the presence of clouds in difficult regions, such as over snow/ice surfaces or in sunglint regions.

   b) Determine cloud macrophysical properties (cloud layer and cloud top pressure) for cloudy pixels (ATBD 4.2). The Release 2 algorithms include the spatial coherence technique, a multispectral technique and the CO_2 slicing technique.

   c) Determine cloud microphysical and optical properties (base and effective radiating center temperature and pressure, phase, particle size, optical depth at 0.65 micron, water/ice path, emittance at 10.8 micron) for cloudy pixels (ATBD 4.3). The Release 2 algorithms include the calculation of aerosol optical depth over ocean and VINT algorithm for cloud macrophysical and microphysical properties.

5. Collect the algorithm output and store on the master pixel structure.

6. Output the pixel cloud properties, update the clear-sky map, and start the next chunk.

7. At the end of the processing, prepare a processing summary report, shutdown the algorithms, and

8. Close the files, and terminate processing.

Figure 4.0-7 provides a static view of the design depicting the divisionof the software into objects. Objects contain data and routines that operate on that data. Input data sets are dealt with in the

InputDataSets object. The objects that deal with the main chunk loop are Chunk, Pixel, and Algorithm Manager. The Algorithm manager is an abstraction of individual managers that prepare algorithm specific input, call the algorithm, and manage results according to the type of algorithm invoked. Similar to the input, OutputDataSets groups the functions to get pixel data from the chunk and output them to the various products and the functions to calculate final statistics for the Quality Control (QC) reports.

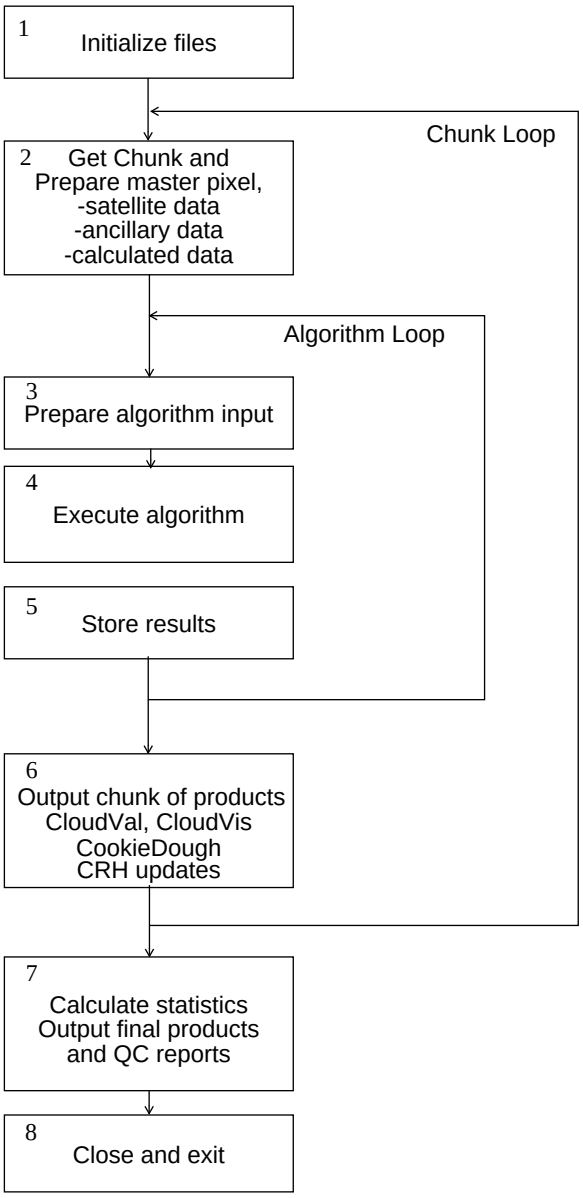

Figure 4.0-6. High-level Cloud Retrieval Flow Chart

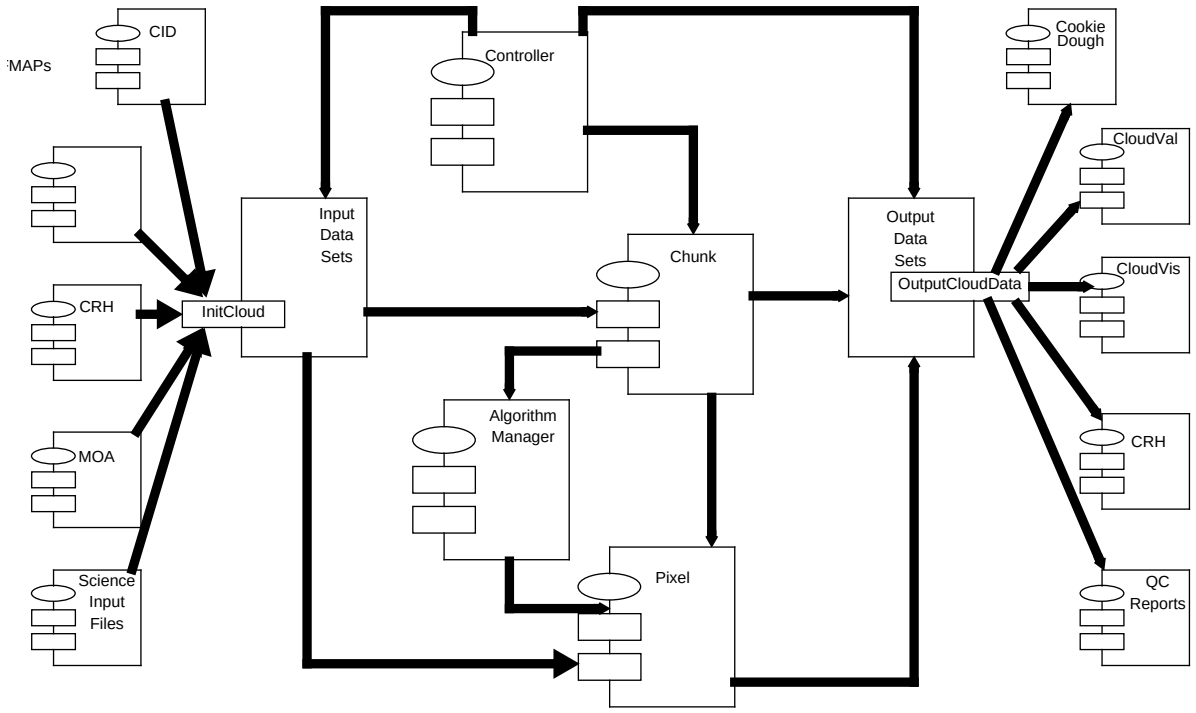

Figure 4.0-7. Design Overview Context Diagram

4.0.7.4 Implementation Constraints

The implementation constraints are the EOSDIS operating environment, the Science Data Production (SDP) Toolkit, the limits of computer CPU, data throughput, network capacity, and system complexity. In addition, it is an EOSDIS requirement that all filenames must be obtained from the Process Control File by using a Toolkit call, and all file opens must be accomplished by using a Toolkit call. Currently some of the input data files are managed by the science algorithms. Correct file names and open statement usage will be handled on a case-by-case basis with the algorithm developer.

The cloud framework is written in FORTRAN 90 and interfaces with science algorithms written in either FORTRAN or C. The science algorithms are contributed code from members of the Cloud Working Group. Therefore, it was necessary to implement the framework around the contributed code and to consider the contributed code as "black boxes." The approach was taken to interface with the science algorithms by preparing tailor-made interfaces to the black boxes.

The Cloud Subsystem needs hourly input files and produces hourly output products for a single Product Generation Executable (PGE). It is assumed that the Planning and Data Production System (PDPS) will not start the cloud processing system until all required input files are available and that the PDPS will stage all input data files needed for the run.

Release 1 was delivered to the LaRC Distributed Active Archival Center early March 1996 and was run within the EOSDIS Interim Release 1 system. The code is designed to process global data from the existing ERBE/AVHRR data from the NOAA-9 spacecraft.

Only common parameters for the hourly products are collected and output in the form of a header record. These metadata include general header information such as instrument, satellite, start data, start time, end data, end time, and processing date and time.

4.0.8. Processing Estimates

Processing resource requirements for the TRMM and EOS-AM data streams have been estimated by scaling the Version 1 satellite imager analysis codes (Subsystems 4.1, 4.2, and 4.3), subsequent convolution with ERBE FOV's (Subsystem 4.4) and finally ERBE inversion to TOA fluxes (Subsystem 4.5).

The CERES cloud retrieval code (Subsystems 4.1, 4.2, and 4.3) has been exercised using several different processing hardware/software scenarios. The CERES libraries and the EOS Toolkit software were implemented under all scenarios. AVHRR and ERBE data are used as surrogates for the eventual cloud imager (VIRS, MODIS) and CERES. The number of AVHRR imager pixels processed per hour is approximately 2.9 million, while we estimate 3.1 million pixels/hour with VIRS and approximately 34 million pixels/hour with MODIS. Five cloud algorithms were implemented for the timing exercises:

a. CERES cloud threshold tests (Subsystem 4.1)

b. Paired histogram classification technique (Subsystem 4.1)

c. Fuzzy logic cloud layer classifier (Subsystem 4.2)

d. Visible Infrared Near-Infrared Technique (VINT) for cloud properties (Subsystem 4.3)

e. Aerosol optical depth retrieval over ocean

The three production scenarios are the following:

1. The production code was exercised using AVHRR 4-km Global Area Coverage data and ERBE data on a Silicon Graphics computer with R8000 CPU's using the NAG 32-bit Fortran 90 compiler and the SGI C compiler. The production code was run in single processor mode so that while multiple CPU's were available, the code ran on only one CPU. The NAG Fortran 90 compiler does not allow for any optimization. The SGI operating system was IRIX 6.0.

   Average wall clock processing time/hour of AVHRR data: 150 minutes

2. Same procedure as in (1) but using the first release of the 64-bit SGI Fortran 90 compiler and an upgraded SGI operating system IRIX 6.2.

   Average wall clock processing time/hour of AVHRR data: 80 minutes

3. Same as (2) but using new R10000 CPU's. Again, the production code was run in single processor mode.

   Average wall clock processing time/hour of AVHRR data: 30 minutes

Given the rapid improvement in microprocessor speeds, workstations will be capable of processing the VIRS and later MODIS data streams faster than real-time. The larger problem may well be data storage. For the MODIS and VIRS data, the Langley DAAC will not keep a separate level 1b archive, but will only keep data for the last month or two to simplify data storage. Any later reprocessing would return to the GSFC DAAC to obtain the required MODIS level 1b data.

4.0.9. Relationship of MODIS and CERES Cloud Data Products

4.0.9.1. Background

One of the comments of the peer review panel was that CERES and MODIS Science Teams are both producing estimates of cloud properties. Is this a duplication of effort? Can't one cloud product satisfy all users?

If we view clouds as large (relative to satellite image pixels), well-defined, and well-behaved sheets of paper floating in the atmosphere, then one cloud definition will suffice for all users. We simply define whether the sheet is present or not, the altitude of cloud occurrence, and the properties of the cloud sheet.

Field experiments show that actual clouds

- Change on time scales of seconds to hours (much less than satellite revisit time)
- Change on space scales from meters to 10, 000 km (much smaller than to much greater than satellite pixel size)
- Have highly variable shapes and configurations
- Occur at least half the time in multiple overlapping cloud layers
- Often have optically thin cloud edges; no sharp cloud/clear boundary (boundary layer clouds)
- Are often sufficiently optically thin to be at the edge of detectability with passive radiometers (cirrus clouds)

Given this extreme variability, and the associated difficulty in accurately remotely sensing cloud properties, it is unlikely that a single approach to cloud measurement will meet all needs.

4.0.9.2. EOS cloud products

In particular there are three major categories of cloud data required: cloud masking, cloud physical properties, and cloud radiative properties. For each of these areas, the MODIS and CERES teams are cooperatively examining a range of strategies to derive cloud properties. A comparison of MODIS and CERES cloud products is given in Table 4.0-2. The table gives the primary *focus* of each product, *not* its only use. The focus, or top priority, however, controls the future processing strategies and adjustments as we learn more about clouds using the EOS and field experiment observations.

Table 4.0-2. Comparison of MODIS and CERES Cloud Products

MODIS: Daytime solar channels (King)	MODIS: Day/night infrared HIRS-like clouds (Menzel)	CERES: Day/night, solar/lnfrared VIRS-like clouds (Barkstrom)
Cloud dynamics	Cloud dynamics	Cloud radiative effects
Daytime only	Daytime and nighttime	Daytime and nighttime
Instantaneous	Time averaged	Time averaged
Pixel to global scale	Regional to global scale	Regional to global scale
Rapid algorithm improvement	Infrequent algorithm improvement	Slow algorithm improvement
Time series inconsistency allowed	Time series must be consistent	Time series must be consistent
Algorithm change MIGHT = Reprocessing	Algorithm change MUST = Reprocessing	Algorithm change MUST = Reprocessing
Subset of cloud properties OK *(all retrieved properties high accuracy)*	Subset of cloud properties OK *(all retrieved properties high accuracy)*	Complete cloud properties required *(some cloud properties low accuracy such as cloud thickness and base)*
Cloud properties stand alone	Cloud properties must be consistent with existing HIRS data	MODIS/VIRS must be consistent *(at least in early years of EOS)*
Avoid marginal cloudy/clear data in time and space averaged data	Include marginal cloudy/clear data in time and space averaged data	Include marginal cloudy/clear data in time and space averaged data

1. Cloud masking: Determination of each satellite pixel as either cloud-free or cloud contaminated.

Masking determines if a satellite pixel is a candidate for use in observing surface properties after correction for atmospheric effects. For example

- SST (sea surface temperature) observations: optically thin boundary layer cloud is acceptable (small thermal infrared impact) while optically thin cirrus is damaging (relatively large thermal infrared effect). Cloud shadows have no effect.
- Vegetation canopy studies: More thin cirrus is allowable, but need to avoid cloud shadows.
- Fields of view which are uncertain (could be clouds or clear) will usually be ignored in MODIS time and space averages of cloud and surface properties. These data will be included in the CERES time and space averages of cloud properties for radiation budget purposes.

2. Cloud physical properties: Cloud property estimates for use in characterizing cloud properties over the globe, and for testing dynamical models of clouds.

Emphasis is on getting accurate cloud water budget: liquid water, ice water, cloud amount, height, and particle size/phase. Statistics in a grid cell, or over a type of cloud, are most critical, since a simulated cloud field can never be expected to match real clouds cell for cell (predictability problem and inadequate model initialization at cloud scale). Primary emphasis is on provision of regional cloud properties with highest accuracy, but availability depends on actual cloud conditions. Secondary emphasis is on global scale properties. As improvements in cloud remote sensing are developed using MODIS, they are implemented, with improvements every 3–6 months shortly after launch and at 1–2 year intervals thereafter. Reprocessing of the previous data is decided on a case by case basis. Accuracy of current data is more important than a single consistent time record.

Cloud properties vary greatly in their effect on solar radiation (scattering dominated) as opposed to thermal infrared radiation (absorption and emission dominated). MODIS will exploit this difference to pursue two different strategies for determining cloud physical properties. One set of cloud data (King; see Table 4.0-1) will focus on information retrieved using solar reflectance channels on MODIS to derive cloud particle size and cloud optical depth during daytime observations. A second set of cloud data (Menzel; see Table 4.0-1) will focus on information retrieved using the thermal infrared channels on MODIS to derive cloud effective emittance, cloud height, and cloud particle size. Each technique has advantages and disadvantages that will be useful in studies of clouds. The thermal infrared cloud data will also extend in time a global cloud data set started using the NOAA HIRS/2 data. For climate record analysis, the infrared cloud analysis technique will be consistent for the HIRS and MODIS data sets.

3. Cloud radiative properties: Cloud property estimates for use in determining the radiation budget at the top of the atmosphere, within the atmosphere, and at the surface, and for studying the role of clouds and radiation in the climate system.

Many studies of cloud/climate feedback mechanisms will require cloud and radiation budget data which are internally consistent. For CERES (Barkstrom; see Table 4.0-1), the emphasis is on radiatively effective cloud data. Emphasis is also on global data available at all times and places. Secondary emphasis is on regional studies. Because climate data must be stable for long periods of time, algorithms are updated very infrequently, perhaps once every 3–5 years. When algorithms are updated, all previous data are reprocessed with the new algorithms. A single consistent time record is of primary importance; accuracy of current data is of secondary importance. As an example, CERES will have flown on the TRMM spacecraft in the year before the launch of EOS-AM. Accurate determination of the diurnal cycle of radiation will require combination of TRMM, EOS-AM, and EOS-PM data. But the TRMM cloud imager (VIRS) is not as capable as the MODIS instrument on EOS-AM and EOS-PM. VIRS has a larger footprint, and has only half of the MODIS channels useful for cloud property analysis. CERES will need to maximize the consistency between VIRS and MODIS cloud properties, thereby

maximizing the time sampling information provided by the TRMM precessing orbit. A trade-off will result; the CERES analysis of MODIS data will strive for consistency with VIRS on the one hand, and full utilization of MODIS on the other. The trade-off will be decided by examining the impact of the decision on derived CERES radiative fluxes. The likely result is that CERES will sacrifice some of the MODIS cloud property accuracy for consistency with TRMM cloud data from VIRS. The MODIS team, in contrast, will seek to utilize the full capability of the MODIS data for cloud physical properties.

4.0.9.3. Data processing cost issues

At a recent workshop on the future projections for computing capabilities in the late 1990's (Skamania, October 1994), two conclusions were reached:

- Flops and baud will be free [i.e., processing power and data transfer rates (bits per second for sequential data transfer) will get very cheap].
- Data storage costs will not fall nearly as fast. Data random access times will also fall much slower.

The conclusion is that in the near future the additional cost of processing data twice in a global streaming mode (e.g. process all data in time-ordered fashion) will be relatively inexpensive. While processing power (Flops) have continued to decrease in cost over the last three years, data transfer rates have yet to significantly decrease. As a result, using the EOSDIS project estimate of a required 75Mbits/sec of bandwidth between GSFC and LaRC (mostly for MODIS data transfer, including reprocessing transfers at several times real-time acquisition rates) it would cost about 2.5 dedicated "T3" lines at roughly $35K/month per T3 line, for a yearly cost of roughly $1M. When the order of magnitude reductions in data transfer rates become a reality, then this would reduce to a reasonable $100K/year requirement.

Meanwhile, the more cost effective option at present is obviously the transfer of data by storage tape. This is especially true for a climate data set like CERES: there is no requirement for near real-time processing: a delay of 1 to 2 months after data acquisition is acceptable. Both the LaRC and GSFC DAACs use juke-boxes with Storage Tek D3 storage tapes as the archive medium. These tapes cost $100 each and hold 50Gbytes of data per tape. In streaming mode, the tape data transfer rate is roughly 10Mbytes/second, so that 50Gbytes can be transferred in roughly 90 minutes. The entire global MODIS level 1b data stream for 1 day is 180Gbytes, of which CERES expects to use a spectral channel subsample of about one-half this data volume, or roughly 90Gbytes/day. Converted onto D3 tapes, 90Gbytes/day is roughly 2 tapes and 3 hours to copy. Each tape drive costs $100K, but both LaRC and GSFC DAACs use these tape drives in their current data archive systems (up to 8 drives per jukebox). A single drive at GSFC could copy 4 days of global level 1b MODIS data per 24hour period in an automated manner (assume a factor of 2 drop in copy speed for write/verify of the copy at GSFC). The only manual intervention would be de-mounting the tapes and shipping to LaRC, then cataloging the tapes on reception at LaRC. Cataloging could be simplified by electronically transferring the information on files copied to each tape. The major cost of this method of transferring 4 tapes per day would be roughly 1/4 workforce-year of effort at GSFC to support catalog/shipping of tapes, and 1/4 workforce-year at LaRC to support catalog/receiving of the tapes. This cost would average $40 to $50K/year. The cost of an extra tape drive at GSFC if necessary would be $100K for the first year, and given a 4 year lifetime for the drive, a yearly average cost of $25K. If a revolving archive of tapes sufficient to hold 3 months of global MODIS data is used for data transfer, the cost of tapes in the beginning is $16K. Final yearly cost during the first 4 years would be expected to average roughly $50K (workforce) + $25K (drive) + $16K (tapes) = $90K/year. At the end of 4 years, electronic transfer might be cost competitive and provide a viable long-term automated data transfer mechanism. Even if data line costs do not drop as expected, the cost of tapes and tape drives would decrease and the yearly cost would be limited by the workforce managing the tape transfer/cataloging function.

4.0.9.4. Summary

The role of clouds and radiation in the climate system is one of the highest priority science issues in the U.S. Global Change Research Program. Solutions to this problem will be very difficult, and therefore should be approached from distinctly different perspectives to maintain program robustness. The cost of processing two different views (dynamical and radiative) of cloud properties using the MODIS data is a very small fraction of the cost of building, flying, and operating the MODIS instrument and processing the data.

Any single cloud algorithm team will be subject to a "one size fits all" approach. This approach will not be optimal for any cloud data use and will suppress new creative solutions to problems. On the other hand, the current uncertainties are sufficiently large that in a room of 12 cloud researchers one is likely to find 12 different proposed cloud algorithms. EOS cannot afford to support all possibilities, but must, however, support a few key strategies best suited to the EOS observational capabilities.

We propose that CERES provide a cloud data set focused on the needs of the cloud radiation budget science issues and that MODIS provide a data set focused on the needs of cloud dynamics and cloud processes science issues.

Note that MODIS and CERES are not the only investigations which will provide critical contributions needed for cloud/climate research. In particular

- MISR will provide unique simultaneous multiangle solar reflectance observations to verify the radiative modeling of inhomogeneous cloud cells and cloud fields. MISR will also provide independent verification of cloud heights using stereo viewing techniques.
- AIRS (Atmospheric Infrared Sounder) will provide unique high spectral resolution infrared observations of clouds that will allow more complete examination of cloud microphysics at night, and a consistent day/night subset of cloud properties.
- ASTER will provide very high spatial resolution data (15–90 m) for verification of the effects of beam filling on global data derived using coarser resolution sensors such as MODIS and VIRS.
- EOSP (Earth Observing Scanning Polarimeter) polarization measurements offer the best hope of distinguishing ice particle shape.
- Eventually, cloud lidar (thin clouds) and cloud radar (thick clouds) will be required to verify the EOS capabilities for overlapped multilevel cloud conditions.

MODIS and CERES provide the two most comprehensive global cloud data sets for global change studies. But there are additional critical contributions made by other instruments that also will be necessary to solve the role of clouds in the climate system.

4.0.9. References

Arking, A.; and Childs, J. D. 1985: Retrieval of Cloud Cover Parameters From Multispectral Satellite. *J. Climat. & Appl. Meteorol.*, vol. 24, pp. 322–333.

Barker, Howard W.; Wielicki, Bruce A.; Parker, Lindsay; 1996: A Parameterization for Computing Grid-Averaged Solar Fluxes for Inhomogeneous Marine Boundary Layer Clouds. Part II; Validation Using Satellite Data. *Journal of the Atmospheric Sciences*, vol. 53, no. 16, pp. 2304-2316.

Baum, Bryan A.; Arduini, Robert F.; Wielicki, Bruce A.; Minnis, Patrick; and Si-Chee, Tsay 1994: Multilevel Cloud Retrieval Using Multispectral HIRS and AVHRR Data: Nighttime Oceanic Analysis. *J. Geophys. Res.*, vol. 99, no. D3, pp. 5499–5514.

Baum, B.A; Uttal, T.; Poellet, M.; Ackerman, T.P.; Alvarez, J; Intrieri, J; Starr, D. O'C; Titlow, J; Tovinkere, V.; and Clothiaux, E. 1995: Satellite remote sensing of multiple cloud layers. *J. Atmos. Sci*., vol 52, no. 23, pp. 4210-4230.

Cahalan, Robert F.; Ridgway, William; Wiscombe, Warren J.; Gollmer, Steven; and Harshvardhan 1994: Independent Pixel and Monte Carlo Estimates of Stratocumulus Albedo. *J. Atmos. Sci.*, vol. 51, no. 24, pp. 3776–3790.

Chambers, L. H., B. A. Wielicki, and K. F. Evans, On the accuracy of the independent pixel approximation for satellite estimates of oceanic boundary layer cloud optical depth. Submitted to *J. Geophys. Res*., April, 1996.

Coakley, J. A., Jr.; and Bretherton, F. P. 1982: Cloud Cover From High-Resolution Scanner Data: Detecting and Allowing for Partially Filled Fields of View. *J. Geophys. Res.*, vol. 87, pp. 4917–4932.

Coakley, J. A., Jr.; and Davies, R. 1986: The Effect of Cloud Sides on Reflected Solar Radiation as Deduced from Satellite Observations. *J. Atmos. Sci.*, vol. 43, pp. 1025–1035.

Coakley, James A., Jr.; Bernstein, Robert L.; and Durkee, Philip A. 1987: Effect of Ship-Stack Effluents on Cloud Reflectivity. *Science*, vol. 237, pp. 1020–1022.

Greenwald, Thomas J.; Stephens, Graeme, L.; Vonder Haar, Thomas H.; and Jackson, Darren L. 1993: A Physical Retrieval of Cloud Liquid Water Over the Global Oceans Using Special Sensor Microwave/Imager (SSM/I) Observations. *J. Geophys. Res.*, vol. 98, no. D10, pp. 18471–18488.

Hahn, C. J.; Warren, S. G.; London, J.; Chervin, R. M; and Jenne, R. 1982: *Atlas of Simultaneous Occurrence of Different Cloud Types Over the Ocean*. NCAR TN-201.

Harshvardhan; Ginger, K.; and Wielicki, B. A. 1994: The Interpretation of Remotely Sensed Cloud Properties From a Model Parameterization Perspective. *Eighth Conference on Atmospheric Radiation*, pp. 443–445.

Jacobowitz, H.; Soule, H. V.; Kyle, H. L.; and House, F. B. 1984: The Earth Radiation Budget (ERB) Experiment—An Overview. *J. Geophys. Res.*, vol. 89, pp. 5021–5038.

King, M. D.; Kaufman, Y. J.; Menzel, W. P.; and Tanre, D. 1992: Remote Sensing of Cloud, Aerosol, and Water Vapor Properties from the Moderate Resolution Imaging Spectrometer (MODIS). *IEEE Trans. Geosci. & Remote Sens.*, vol. 30, no. 1, pp. 2–27.

Lin, X.; and Coakley, J. A., Jr. 1993: Retrieval of Properties for Semitransparent Clouds From Multispectral Infrared Imagery Data. *J. Geophys. Res.*, vol. 98, pp. 18,501–18,514.

Lin, Bing; Minnis, P.; and B. A. Wielicki; 1997b: Estimation of water cloud properties from satellite microwave and optical measurements in oceanic environments. II: Results. Submitted to *Journal of Geophysical Research.*

Lin, Bing; Wielicki, B. A.; Minnis, P.; and Rossow, W; 1997a: Estimation of water cloud properties from satellite microwave and optical measurements in oceanic environments. I: Microwave brightness temperature simulations. Submitted to J*ournal of Geophysical Research.*

Loeb, Norman G.; Varnai, Tamas; Winker, David M; 1997: Influence of Sub-pixel Scale Cloud-Top Structure on Reflectances from Overcast Stratiform Cloud Layers. Submitted to the *Journal of the Atmospheric Sciences.*

Luo, G.; Lin, X.; and Coakley, J. A. 1994: 11-μm Emissivities and Droplet Radii for Marine Stratocumulus. *J. Geophys. Res.*, vol. 99, pp. 3685–3698.

Minnis, Patrick; Heck, Patrick W.; and Young, David 1993: Inference of Cirrus Cloud Properties Using Satellite-Observed and Infrared Radiances. Part II: Verification of Theoretical Cirrus Radiative Properties. *J. Atmos. Sci.*, vol. 50, no. 9, p. 1322.

Nagarajarao, C. R., ed. 1993: *Degradation of the Visible and Near-Infrared Channels of the Advanced Very High Resolution Radiometer on the NOAA-9 Spacecraft—Assessment and Recommendations for Corrections*. NOAA-TR-NESDIS-70.

Payette, F. 1989: Application of a Sampling Strategy for the ERBE Scanner Data. M.S. Thesis, McGill Univ.

Rossow, William B. 1989: Measuring Cloud Properties From Space—A Review. *J. Climat.*, vol. 2, pp. 201–213.

Rossow, William B.; Garder, Leonid, C.; Lu, Pei-Jane; and Walker, Alison 1992: *International Satellite Cloud Climatology Project (ISCCP): Documentation of Cloud Data*. World Meteorol. Org.

Sheu, R.-S.; Curry, J. A.; and Liu, G.; 1996: Vertical stratification of tropical cloud properties as determined from satellite. Submitted to *J. Geophys. Res*.

Staylor, W. Frank 1990: Degradation Rates of the AVHRR Visible Channel for the NOAA 6, 7, and 9 Spacecraft. *J. Atmos. & Ocean. Technol.*, vol. 7, pp. 411–423.

Stackhouse, P. W.; and Stephens, G. L. 1994: Investigation of the Effects of Macrophysical and Microphysical Properties of Cirrus Clouds on the Retrieval of Optical Properties—Result from FIRE II. *Eighth Conference on Atmospheric Radiation*, pp. 225–227.

Stephens, Graeme L. 1988: Radiative Transfer Through Arbitrarily Shaped Optical Media. II—Group Theory and Simple Closures. *J. Atmos. Sci.*, vol. 45, pp. 1818–1848.

Stephens, G. L.; Paltridge, G. W.; and Platt, C. M. R. 1978: Radiation Profiles in Extended Water Clouds. III—Observation. *J. Atmos. Sci.*, vol. 35, pp. 2133–2141.

Stowe, L. L.; Wellemeyer, C. G.; Eck, T. F.; and Yeh, H. Y. M.; and Nimbus-7 Cloud Data Processing Team 1988: Nimbus-7 Global Cloud Climatology. I—Algorithms and Validation. *J. Climat*., vol. 1, no. 5, pp. 445–470.

Suttles, J. T.; Green, R. N.; Minnis, P.; Smith, G. L.; Staylor, W. F.; Wielicki, B. A.; Walker, I. J.; Young, D. F.; Taylor, V. R.; and Stowe, L. L. 1988: *Angular Radiation Models for Earth-Atmosphere System. Volume I: Shortwave Radiation*. NASA RP-1184.

Suttles, John T.; Wielicki, Bruce A.; and Vemury, Sastri 1992: Top-of-Atmosphere Radiative Fluxes—Validation of ERBE Scanner Inversion Algorithm Using Nimbus-7 ERB Data. *J. Appl. Meteorol.*, vol. 31, no. 7, pp. 784–796.

Takano, Yoshihide; and Liou, Kuo-Nan 1989: Solar Radiative Transfer in Cirrus Clouds. I—Single-Scattering and Optical Properties of Hexagonal Ice Crystals. *J. Atmos. Sci.*, vol. 46, pp. 3–36.

Tian, Lin; and Curry, Judith A. 1989: Cloud Overlap Statistics. *J. Geophys. Res.*, vol. 94, pp. 9925–9935.

Taylor, V. Ray; and Stowe, Larry L. 1984: Reflectance Characteristics of Uniform Earth and Cloud Surfaces Derived from NIMBUS 7 ERB. *J. Geophys. Res.*, vol. 89, no. D4, pp. 4987–4996.

Wang, J. and Rossow, W. B.; 1995: Determination of cloud vertical structure from upper-air observations. *J. Appl. Met*., vol. 34, pp. 2243-2258.

Warren, S. G.; Hahn, C. J.; and London, J. 1985: Simultaneous Occurrence of Different Cloud Types. *J. Climat. and Appl. Meteorol.*, vol. 24, pp. 658–667.

Welch, Ronald M.; Cox, Stephen K.; and Davis, John M. 1980: Solar Radiation and Clouds. *Meteorol. Monogr*., vol. 17, no. 39.

Wielicki, Bruce A.; and Green, Richard N. 1989: Cloud Identification for ERBE Radiative Flux Retrieval. *J. Appl. Meteorol.*, vol. 28, pp. 1133–1146.

Wielicki, Bruce A.; Barkstrom, B. R.; Harrison, E. F.; Lee III R. B.; Smith G. L.; and Cooper, J. E. 1996: Clouds and the Earth's Radiant Energy System (CERES)—An Earth Observing System Experiment. *Bulletin of the American Meteorological Society*, vol. 77, no. 5, pp. 853-868.

Wielicki, Bruce A.; and Parker, Lindsay 1992: On the Determination of Cloud Cover from Satellite Sensors—The Effect of Sensor Spatial Resolution. *J. Geophys. Res.*, vol. 97, no. D12, pp. 12799–12823.

Wielicki, B. A.; and Welch, R. M. 1986: Cumulus Cloud Properties Derived Using Landsat Satellite Data. *J. Climat. & Appl. Meteorol.*, vol. 25, pp. 261–276.

Ye, Qian 1993: The Spatial-Scale Dependence of the Observed Anisotropy of Reflected and Emitted Radiation. PH.D Diss., Ohio State Univ.

Appendix A - Input Data Products

Determine Cloud Properties, TOA and Surface Fluxes (Subsystem 4)

This appendix describes the data products which are used by the algorithms in this subsystem. The table below summarizes these products, listing the CERES and EOSDIS product codes or abbreviations, a short product name, the product type, the production frequency, and volume estimates for each individual product as well as a complete data month of production. The product types are defined as follows:

Archival products:	Assumed to be permanently stored by EOSDIS
Internal products:	Temporary storage by EOSDIS (days to years)
Ancillary products:	Non-CERES data needed to interpret measurements

The following pages describe each product. An introductory page provides an overall description of the product and specifies the temporal and spatial coverage. The table which follows the introductory page briefly describes every parameter which is contained in the product. Each product may be thought of as metadata followed by data records. The metadata (or header data) is not well-defined yet and is included mainly as a placeholder. The description of parameters which are present in each data record includes parameter number (a unique number for each distinct parameter), units, dynamic range, the number of elements per record, an estimate of the number of bits required to represent each parameter, and an element number (a unique number for each instance of every parameter). A summary at the bottom of each table shows the current estimated sizes of metadata, each data record, and the total data product. A more detailed description of each data product will be contained in a User's Guide to be published before the first CERES launch.

Table A-1. Input Products Summary

Product Code		Name	Type	Frequency	Size, MB	Monthly Size, MB
CERES	EOSDIS					
CID_MODIS	CERX04	MODIS Cloud Imager Data	Ancillary	1/2.5	167.8	2,997,426
CID_VIRS	CERX05	VIRS Cloud Imager Data	Ancillary	1/Hour	57.33	42,653
CRH	CER16	Clear Reflectance History	Archival	Every 10 Days	91.1	282
IES	CER09	Instrument Earth Scans	Internal	1/Hour	35.7	26,561
MOA	CERX06	Meteorological, Ozone and Aerosols	Archival	1/Hour	11.55	8,591
SURFMAP	CERX07	Surface Map	Ancillary	1/Week	13.35	54

MODIS Cloud Imager Data (CID_MODIS)

CID_MODIS (MODIS Cloud Imager Data) is a level-1B data set from the EOS spacecraft with eleven of the MODIS channels. The file is in HDF. At this time, the organizational and content details of this product are not finalized.

The MODIS cloud imager data (CID_MODIS) from the EOS spacecraft is level 1b data from 11 of the MODIS channels. The data coverage is 1 hour. The product has a header record followed by multiple scan line records. The organizational details of this product are not finalized yet. Each pixel in the scan line record has radiance values for each of the channels. In addition, each scan line record contains time, location, and solar angle data. It is assumed that the data are organized in the scan lines that appear to scan in the same direction for each scan.

The channels requested by the CERES Science Team are

MODIS Channels	Central Wavelength (microns)	Resolution (km)
1	0.645	0.25 & 1
6	1.64	1
7	2.13	1
17	0.91	1
18	0.93	1
19	0.94	1
20	3.75	1
23	4.0	1
24	4.46	1
25	4.52	1
26	1.38	1
27	6.7	1
29	8.55	1
31	11.0	1
32	12.0	1
33	13.3	1
34	13.6	1
35	13.9	1
36	14.2	1

The CERES Science Team has requested averaged data from the 1/4-km resolution channel to 1 km, and the two 1/2-km resolution channels averaged to 1-km resolution. The team is currently considering further whether to also ingest the full-resolution (0.25-km) channel 1 data. The cloud sytem thus requires input data from the 19 channels .

The CID_MODIS product is external to the CERES processing and is released after CERES processing is completed. It is assumed that the responsible EOSDIS DAAC would retain a copy of this product should it be needed by CERES for a rerun.

Level: 1-B
Type: Ancillary
Frequency: 1/2.5min

Portion of Globe Covered
File: Satellite Swath

Time Interval Covered
File: 2.5 min

Portion of Atmosphere Covered
File: Satellite Altitude

Table A-2. MODIS Cloud Imager Data (CID_MODIS) Page 1 of 1

Description	Parameter Number	Units	Range	Elements/ Record	Bits/ Elem
CID_MODIS					
MODIS HDF Header					
ECS Standard Granule Metadata		N/A	N/A	1	
Level 1B Non-core Granule Metadata		N/A	N/A	1	
Level 1B Granule Specific Metadata		N/A	N/A	1	
Level 1B Swath Metadata		N/A	N/A	1	544
Level 1B Instrument Data: Dimensions		N/A	N/A	1	1376
Level 1B Instrument Data: Slopes and Offsets		N/A	N/A	1	5632
MODIS HDF Data					
250 M SDS (1 Channel)					
EV_250_RefSB_Rad	2	N/A	N/A	21,664,000	32
500 M SDS (2 Channels)					
EV_500_RefSB_Rad	7	N/A	N/A	10,832,000	32
1000 M SDS (8 Channels)					
EV_1000_RefSB_Rad	13	N/A	N/A	10,832,000	32
Geolocation Data					
Latitude	29			135,400	32
Longitude	30			135,400	32
Solar Zenith	31			135,400	32
Azimuthal	32			135,400	32
Viewing Zenith	33			135,400	32

Total Meta Bits/File:	7,552
Total Data Bits/File:	1,408,160,000
Total Bits/File :	1,408,167,552
Total Mbytes/File:	168

VIRS Cloud Imager Data (CID_VIRS)

The VIRS Cloud Imager Data (CID_VIRS) are level 1-B data from the five VIRS channels on the TRMM spacecraft. The data coverage is one orbit; however, the orbit files will be processed on an hourly basis. The sizes listed in the following data description reflect the number of scan line records in one hour (11,808). The product is in Hierarchical Data Format (HDF). The product contains metadata and various HDF structures which hold the geolocation data, spacecraft navigation data, local direction angles to the sun and the spacecraft, scan status data, imager calibration data, and imager radiance data for all of the scan line records. All radiance values for a single channel for all scan lines are together in the same HDF structure. It is assumed that the data are organized in scan lines that appear to scan in the same direction for each scan.

The VIRS product contains the following types of data :

Metadata	Spacecraft navigation data
HDF swath structure	Calibration data
Scan Time	Local direction angles to sun and satellite
Pixel geolocation	VIRS imager pixel data
Scan status flags	

The channels from VIRS are :

Channels	micron	Resolution
Channel 1	0.63	2 km
Channel 2	1.60	2 km
Channel 3	3.75	2 km
Channel 4	10.80	2 km
Channel 5	12.00	2 km

CID_VIRS products are external to the CERES processing and are released after CERES processing is completed. It is assumed that the responsible EOSDIS DAAC would retain a copy of this product should it be needed by CERES.

Level: 1-B
Type: Ancillary
Frequency: 1/Hour

Portion of Globe Covered
File: Satellite Swath

Time Interval Covered
File: 1 Hour

Portion of Atmosphere Covered
File: Satellite Altitude

Table A-3. VIRS Cloud Imager Data (CID_VIRS) Page 1 of 1

Description	Parameter Number	Units	Range	Elements/ Record	Bits/ Elem
CID_VIRS					
VIRS Metadata					
ECS Core Metadata		N/A	N/A	1	80000
Product Specific Metadata		N/A	N/A	1	80000
VIRS Swath Data					
Swath Structure for HDF					
HDF information for decoding the product	1	N/A	TBD	1	40000
Scan Time is Array[11808] of:					
UTC seconds of day	2	sec	TBD	11808	64
Geolocation is Array[11808] of:					
Pixel Location is Array[261] of:					
Latitude of imager pixel	3	deg	-90 .. 90	3081888	32
Longitude of imager pixel	4	deg	0..360	3081888	32
Scan Status is Array[11808] of:					
Scan status	5	N/A	TBD	11808	152
Navigation is Array[11808] of:					
Spacecraft Geocentric Position is					
x component	6	m	TBD	11808	32
y component	7	m	TBD	11808	32
z component	8	m	TBD	11808	32
Spacecraft Geocentric Velocity is					
xdot component	9	m sec^{-1}	TBD	11808	32
ydot component	10	m sec^{-1}	TBD	11808	32
zdot component	11	m sec^{-1}	TBD	11808	32
Spacecraft Geodetic Position is					
Latitude	12	deg	-90 .. 90	11808	32
Longitude	13	deg	0..360	11808	32
Altitude	14	m	TBD	11808	32
Spacecraft Geocentric Attitude is Array[3] of:					
yaw, pitch, roll	15	deg	TBD	35424	32
Sensor Orientation Matrix is Array[9] of:					
Instrument coordinate rotation to Geocentric Inertial Coordinates	18	N/A	TBD	106272	32
Greenwich Hour Angle	19	deg	TBD	11808	32
Calibration Counts is Array[11808] of:					
Channel Number/Data Word is Array[5,2] of:					
Blackbody	20	count	TBD	118080	16
Spaceview	21	count	TBD	118080	16
Solar Diffuser	22	count	TBD	118080	16
Local Direction is Array[11808] of:					
Pixel Number is Array[27] of:					
Zenith angles to the satellite	23	deg	0 .. 90	318816	16
Zenith angles to the sun	24	deg	0 .. 90	318816	16
Azimuth angles to the satellite	25	deg	0 .. 90	318816	16
Azimuth angles to the sun	26	deg	0 .. 90	318816	16
Image Data is Array[11808] of:					
Channel Data is Array[261] of:					
Channel 1, .63 micrometers (visible), day only	27	mW cm^{-2} um^{-1} sr^{-1}	TBD	3081888	16
Channel 2, 1.6 micrometers (near infrared), day only	28	mW cm^{-2} um^{-1} sr^{-1}	TBD	3081888	16
Channel 3, 3.75 micrometers (infrared), day and night	29	mW cm^{-2} um^{-1} sr^{-1}	TBD	3081888	16
Channel 4, 10.7 micrometers (infrared, clouds), day and night	30	mW cm^{-2} um^{-1} sr^{-1}	TBD	3081888	16
Channel 5, 12.0 micrometers (infrared, moisture), day and night	31	mW cm^{-2} um^{-1} sr^{-1}	TBD	3081888	16

Total Metadata Bits/File:	160 000
Total HDF Swath Structure Bits/File:	40 000
Total Data Bits/File:	480 727 296
Total Bits/File:	480 927 296
Total Megabytes/File:	57.33

Clear Reflectance History (CRH)

The Clear Reflectance/Temperature History (CRH) data are organized on a global equal-area grid that is approximately 1/6 Degree by 1/6 Degree. The data coverage is 24 hours, and is updated every 10 days. The data product consists of a product header followed by fixed-length records organized according to the grid pattern. Each record has:

Visible albedo
Temperature
Viewing angles

The parameters are derived from cloud imager measurements by Subsystem 4. The CRH product is the same structure for both MODIS values and VIRS values. There is a source indication on the header record.

The CRH is archived, therefore, the CERES investigator will have access to any particular day throughout the life of the mission. Also, the product is needed for reprocessing.

Level: 3
Type: Archival
Frequency: Every 10 Days

Portion of Globe Covered
File: Entire Globe
Record: 1/6 Degree by 1/6 Degree

Time Interval Covered
File: Life of Mission
Record: Every 10 Days

Portion of Atmosphere Covered
File: Surface Reference

Table A-4. Clear Reflectance History (CRH) Page 1 of 1

Description	Parameter Number	Units	Range	Elements/Bits/Elem Record	Elem	Num
CRH						
CRH header record		N/A	N/A	1	2048	
Record_CRH is Array[4341600] of:						
Grid_CRH						
Day of observation	1	day	Mission Life	1	321	
Time of observation	2	day	0..1	1	322	
Visible albedo for collimated, overhead sun illumination	3	N/A	0 .. 1	1	163	
Temperature derived from 3.7 μm imager channel	4	K	TBD	1	164	
Temperature derived from 11 μm imager channel	5	K	TBD	1	165	
Solar zenith angle from imager	6	deg	0 .. 90	1	166	
Mean imager viewing zenith over CERES FOV	7	deg	0 .. 90	1	167	
Mean imager relative azimuth angle over CERES FOV	8	deg	0 .. 360	1	168	
Narrowband ADM Type	9	N/A	TBD	1	169	

Total Meta Bits/File:	2048
Total Data Bits/Record:	176
Total Records/File:	4341600
Total Data Bits/File:	764121600
Total Bits/File :	764123648

Instrument Earth Scans (IES)

The IES data product contains the equivalent of one hour of data from a single CERES scan. The data records are spatially ordered along the orbital ground track, with each footprint position related to the spacecraft's suborbital point at the start of the hour. The spatial ordering of records within this product will ease the comparison of CERES data with cloud imager data in subsystem 4.4. The footprint record is the basic data structure for this data product. This record contains the following kinds of information:

1. Time of Observation
2. Geolocation data (at both the Top of Atmosphere (TOA) and at the Earth's surface)
3. Filtered radiances (at satellite altitude), with associated quality data
4. Spacecraft orbital data
5. Footprint viewing geometric data

The IES data product contain only measurements that view the Earth. For the TRMM mission, this means that approximately 225 Earth-viewing footprints (records) are stored on the IES for each 3.3 second half-scan. Because the Earth scan pattern of the CERES instrument in the biaxial scan mode is irregular, the exact number of pixels in each IES data product varies. This variation is caused by the asynchronous scan azimuth position at both the start and end of the hour. If the azimuth angle near the start (or end) of an hour is near the crosstrack position, then the number of footprints in the IES product is near the estimated value given below. If the azimuth angle is near the alongtrack position, some of the footprints are instead spatially located within the previous (or next) hour's IES. Thus, we have used an estimate of the number of 3.3 second half-scans per hour (approximately 1091) times the number of Earth-viewing measurements in a half-scan (TRMM estimate is 225, EOS estimate is 195) to arrive at the IES product size. For TRMM, this is estimated as 245475 measurements per IES data product and for EOS the estimate is 212745 measurements. The larger of these two measures is used to determine product storage sizing.

Level: 1b
Type: Internal
Frequency: 1/Hour

Time Interval Covered
File: 1 Hour
Record: 100 Hz

Portion of Globe Covered
File: Satellite Swath
Record: One CERES footprint

Portion of Atmosphere Covered
File: Satellite Altitude

IES Metadata - TBD

IES Vdatas

The IES product currently contains two HDF Vdatas. The primary Vdata nominally contains an hourly collection of Footprint records sorted by time. The sceond Vdata serves as an sort index for the Footprint table, allowing Footprint records to be retrieved in a sorted manner by Along Track angle. The two IES Vdatas are summarized in Table B-12.

Table A-5. IES Vdata Summary

Vdata Name	Total Records	Fields Per Record	Record Size (bytes)	Fields	~Nominal Size (MB)*
Footprints	~260,000	30	136	See Table B-13	33.72
Along Track Sort Index	~260,000	2	8	See Table B-14	1.98
VDATA TOTAL SIZE					35.70

Table A-6. Footprint Record

Field No.	Field Name / Parameter	Data Type	Units	Range	No. of Components
1	Colatitude at TOA	32 Bit Float	degrees	0.0..180.0	1
2	Longitude at TOA	32 Bit Float	degrees	0.0..360.0	1
3	Colatitude at Surface	32 Bit Float	degrees	0.0..180.0	1
4	Longitude at Surface	32 Bit Float	degrees	0.0..360.0	1
5	Viewing Zenith Angle	32 Bit Float	degrees	0.0..90.0	1
6	Solar Zenith Angle	32 Bit Float	degrees	0.0..180.0	1
7	Relative Azimuth Angle	32 Bit Float	degrees	0.0..360.0	1
8	Azimuth Viewing Angle North	32 Bit Float	degrees	0.0..360.0	1
9	Crosstrack Angle	32 Bit Float	degrees	-90.0..90.0	1
10	Along Track Angle	32 Bit Float	degrees	0.0..360.0	1
11	Cone Angle	32 Bit Float	degrees	0.0..180.0	1
12	Clock Angle	32 Bit Float	degrees	0.0..180.0	1
13	Cone Angle Rate	32 Bit Float	deg sec^{-1}	-100.0..100.0	1
14	Clock Angle Rate	32 Bit Float	deg sec^{-1}	-10.0..10.0	1
15	Satellite Velocity X	64 Bit Float	km sec^{-1}	-10.0..10.0	1
16	Satellite Velocity Y	64 Bit Float	km sec^{-1}	-10.0..10.0	1
17	Satellite Velocity Z	64 Bit Float	km sec^{-1}	-10.0..10.0	1
18	Radius from Earth	64 Bit Float	km	6000.0..8000.0	1
19	Total Filtered Radiance	32 Bit Float	W m^{-2} sr^{-1}	0.0..700.0	1
20	SW Filtered Radiance	32 Bit Float	W m^{-2} sr^{-1}	-10.0..510.0	1
21	LW Filtered Radiance	32 Bit Float	W m^{-2} sr^{-1}	0.0..50.0	1
22	Colatitude of Satellite	32 Bit Float	degrees	0.0..180.0	1
23	Longitude of Satellite	32 Bit Float	degrees	0.0..360.0	1
24	Colatitude of Sun	32 Bit Float	degrees	0.0..180.0	1
25	Longitude of Sun	32 Bit Float	degrees	0.0..360.0	1
26	Earth-Sun Distance	32 Bit Float	AU	0.98..1.02	1
27	Sample Number	U16 Integer	N/A	1..660	1
28	Quality Flags	U32 Integer	N/A	N/A	1
29	Scan Number	U16 Integer	N/A	1..26000	1

Table A-6. Footprint Record

Field No.	Field Name / Parameter	Data Type	Units	Range	No. of Components
30	Observation Time	64 Bit Float	Julian Frac	N/A	1

Table A-7. Along Track Angle Sort Index

Field No.	Field Name	Data Type	Units	Range	No. of Components
1	Footprint Index	U32 Integer	N/A	0..n	1
2	Along Track Angle	32 Bit Float	degrees	0.0..360.0	1

Meteorological, Ozone, and Aerosols (MOA)

The CERES archival product Meteorological, Ozone, and Aerosol Data (MOA) is produced by the CERES Regrid MOA Subsystem. Each MOA file contains meteorological, ozone, and aerosol data for one hour, and is used by several of the CERES subsystems. Data on the MOA are derived from several data sources external to the CERES system, such as the Data Assimilation Office (DAO), NOAA, and various other meteorological satellites. These data arrive anywhere from four times daily to once a month, and have various horizontal resolutions. The Regrid MOA Subsystem interpolates the aerosol and ozone data horizontally to conform with the horizontal resolution of the meteorological data. Profile data are interpolated vertically to conform with CERES requirements. All data are temporally interpolated to provide data to the CERES processing system on an hourly basis.

The MOA contains:

- Surface pressure, geopotential height, skin temperature, and sea surface state
- Vertical profiles of temperature and humidity for 58 atmospheric levels
- Vertical profiles for 18 atmospheric levels below the tropopause of wind u-vector and v-vector data
- Tropospheric height
- Air mass index
- Column precipitable water based on humidity profiles
- Column precipitable water based on microwave measurements
- Column averaged relative humidity
- Vertical profile of ozone mixing ratios for 58 atmospheric levels
- Column ozone
- Aerosol optical depth

Level: 3
Type: Archival
Frequency: 1/Hour

Time Interval Covered
File: 1 hour
Record: 1 hour

Portion of Globe Covered
File: Global
Record: One region

Portion of Atmosphere Covered
File: Surface to TOA

Table A-8. Meteorological, Ozone, and Aerosols (MOA) Page 1 of 1

Description	Parameter Number	Units	Range	Elements/ Record	Bits/Elem ElemNum
Header					
Date and Hour		N/A	ASCII string	1	216
MOA Processing Date		N/A	ASCII string	1	216
MOA Grid Index		N/A	1 .. 1	1	16
Number of MOA Regions		N/A	13104 .. 13104	1	32
Temperature, Humidity, and Ozone Profile Fixed Pressure Levels		hPa	0 .. 1100	55	32
Wind Speed Profile Pressure levels		hPa	0 .. 1100	18	32
Surface Data					
MOA Region Number	1	N/A	1 .. 13104	1	321
Surface Pressure	2	hPa	0 .. 1100	1	322
Surface Geopotential Height	3	m	-100 .. 10000	1	323
Surface Skin Temperature	4	K	175 .. 375	1	324
Flag, Sea Surface State	5	N/A	0 .. 9	1	325
Flag, Source Surface Data	6	N/A	TBD	1	326
Meteorological Profiles					
Temperature Profiles	7	K	175 .. 375	58	327
Specific Humidity Profiles	8	N/A	0 .. 100	58	3265
Wind Profile, U-Vector	9	m sec^{-1}	-100 .. 100	18	32123
Wind Profile, V-Vector	10	m sec^{-1}	-100 .. 100	18	32141
Flag, Source Meteorological Profiles	11	N/A	TBD	1	32159
Meteorological Column Data					
Tropospheric Height	12	hPa	150 .. 300	1	32160
Air Mass Index	13	N/A	0 .. 10	1	32161
Precipitable Water	14	cm	0.001 .. 10.000	1	32162
Column Averaged Relative Humidity	15	N/A	0 .. 100	1	32163
Microwave Precipitable Water	16	cm	0.001 .. 10.000	1	32164
Microwave Precipitable Water, std	17	cm	TBD	1	32165
Flag, Source Microwave Column Precipitable Water	18	N/A	TBD	1	32166
Ozone Profile Data					
Ozone Mixing Ratio Profiles	19	g kg^{-1}	0.00002 .. 0.02	58	32167
Flag, Source Ozone Profile Data	20	N/A	TBD	1	32225
Column Ozone					
Column Ozone	21	du	0 .. 500	1	32226
Flag, Source Column Ozone	22	N/A	TBD	1	32227
Total Column Aerosol					
Optical Depth, Total Column	23	g m^{-2}	0 .. 2	1	32228
Flag, Source Optical Depth, Total Column	24	N/A	TBD	1	32229
Spares	25	N/A	TBD	2	32230

Total Header Bits/File:	544
Total Data Bits/Record:	7392
Total Records/File:	13104
Total Data Bits/File:	96864768
Total Bits/File:	96865312

Surface Map (SURFMAP)

The surface map (SURFMAP) product is a composite product of different types of surface conditions, arranged on a global 1/6 Degree by 1/6 Degree equal-angle grid. The individual products received from different non-EOS sources are

SURFMAP(ICE)	Ice map
SURFMAP(SNOW)	Snow map
SURFMAP(DEM)	Digital Elevation Map
SURFMAP(ECO)	Ecosystem map
SURFMAP(H2O)	Percent water content map
SURFMAP(ERBE)	ERBE Scene id map

The surface type indicator specifies which of the surface conditions best describes the grid cell (land, water, snow, or ice). Snow/ice takes precedence over land/water.

The SURFMAP products are updated at different frequencies, depending on the type of data. For example, the snow and ice map are updated weekly, whereas the elevation map may be used for the life of the mission. EOSDIS will provide the data for some of the required surface conditions. Upon availability and suitability, the CERES software will access these data sets through the Toolkit.

Level: 3
Type: Ancillary
Frequency: Weekly

Time Interval Covered
File: 1 Week
Record: 1 Week

Portion of Globe Covered
File: Entire globe
Record: 1/6 Degree by 1/6 Degree

Portion of Atmosphere Covered
File: Surface

Table A-9. Surface Map (SURFMAP) Page 1 of 1

Description	Parameter Number	Units	Range	Elements/ Record	Bits/ Elem
SURFMAP					
ICE					
Record_ICE is Array[2332800] of:					
Ice map	1	percent	0 .. 100	1	8
SNOW					
Record_SNOW is Array[2332800] of:					
Snow map	2	percent	0 .. 100	1	8
DEM					
Record_DEM is Array[2332800] of:					
Digital Elevation Model	3	km	-12..10	1	16
ECO					
Record_ECO is Array[2332800] of:					
Ecosystem map	4	N/A	0..13	1	8
H2O					
Record_H2O is Array[2332800] of:					
Water map	5	percent	0 .. 100	1	8
ERBE					
Record_ERBE is Array[2332800] of:					
ERBE Scene ID map	6	N/A	1 .. 5	1	8

Total Data Bits/Record:	18,662,400
Total Records/File:	6
Total Bits/File:	111,974,400
Total MBytes/File:	14

Appendix B - Output Data Products

Determine Cloud Properties, TOA and Surface Fluxes (Subsystem 4)

This appendix describes the data products which are produced by the algorithms in this subsystem. The table below summarizes these products, listing the CERES and EOSDIS product codes or abbreviations, a short product name, the product type, the production frequency, and volume estimates for each individual product as well as a complete data month of production. The product types are defined as follows:

Archival products:	Assumed to be permanently stored by EOSDIS
Internal products:	Temporary storage by EOSDIS (days to years)

The following pages describe each product. An introductory page provides an overall description of the product and specifies the temporal and spatial coverage. The table which follows the introductory page briefly describes every parameter which is contained in the product. Each product may be thought of as metadata followed by data records. The metadata (or header data) is not well-defined yet and is included mainly as a placeholder. The description of parameters which are present in each data record includes parameter number (a unique number for each distinct parameter), units, dynamic range, the number of elements per record, an estimate of the number of bits required to represent each parameter, and an element number (a unique number for each instance of every parameter). A summary at the bottom of each table shows the current estimated sizes of metadata, each data record, and the total data product. A more detailed description of each data product will be contained in a User's Guide to be published before the first CERES launch.

Table B-1. Output Products Summary

Product Code		Name	Type	Frequency	Size, MB	Monthly Size, MB
CERES	EOSDIS					
SSF	CER11	Single Satellite Foot-print, and Surface Flux, Clouds	Archival	1/Hour	237.6	176775

Single Satellite Footprint, TOA and Surface Flux, Clouds (SSF)

The Single Satellite CERES Footprint TOA and Surface Fluxes, Clouds (SSF) is produced from the cloud identification, convolution, inversion, and surface processing for CERES. Each SSF covers a single hour swath from a single CERES scanner (3 channels) mounted on one satellite. The product has a product header and multiple records of 113 parameters or 261 elements for each footprint.

The major categories of data output on the SSF are

- CERES footprint geometry and CERES viewing angles
- CERES footprint radiance and flux (TOA and Surface)
- CERES footprint area statistics and imager viewing angles
- CERES footprint clear area statistics
- CERES footprint cloudy area statistics for two out of four cloud height categories
  - Visible optical depth (mean and standard deviation)
  - Logarithm of visible optical depth (mean and standard deviation)
  - Infrared emissivity (mean and standard deviation)
  - Liquid water path (mean and standard deviation)
  - Ice water path (mean and standard deviation)
  - Cloud top pressure (mean and standard deviation)
  - Cloud effective pressure (mean and standard deviation)
  - Cloud effective temperature (mean and standard deviation)
  - Cloud effective height (mean and standard deviation)
  - Cloud bottom pressure (mean and standard deviation)
  - Water particle radius (mean and standard deviation)
  - Ice particle effective diameter (mean and standard deviation)
  - Particle phase (mean and standard deviation)
  - Vertical aspect ratio (mean and standard deviation)
  - Visible optical depth and IR emissivity (13 percentiles)
- CERES footprint cloud overlap conditions (4 conditions)

The SSF is an archival product that will be run daily in validation mode starting with the TRMM launch until sufficient data have been collected and analyzed to produce a production quality set of CERES Angular Distribution Models (CADM). It is estimated that at TRMM launch plus 18 to 24 months, the SSF product will be produced on a routine basis and will be archived within EOSDIS for distribution to the science community.

Level: 2
Type: Archival
Frequency: 1/Hour
Time Interval Covered
File: 1 Hour
Record: 1/100 Second

Portion of Globe Covered
File: Satellite Footprints
Record: One Footprint
Portion of Atmosphere Covered
File: Surface to TOA

Table B-1. Single Satellite Footprint (SSF) Page 1 of 3

Description	Parameter Number	Units	Range	Elements/Record	Bits/Elem	Product Code
SSF						
SSF_Header						
1 Day and Time at hour start		N/A	ASCII string	1		216A
2 Character name of satellite		N/A	ASCII string	1		64A
3 Character name of CERES instrument		N/A	ASCII string	1		32A
4 Character name of high resolution imager instrument		N/A	ASCII string	1		64A
5 Number of imager channels used		N/A	1 .. 20	1		16A
6 Central wavelengths of imager channels		µm	0.4 .. 15.0	20		32A
7 Earth-Sun distance		AU	0.98 .. 1.02	1		32A
8 Day and Time IES processed (SS1.0)		N/A	ASCII string	1		152V
9 Day and Time Imager Cloud properties processed (SS4-1 - 4.3)		N/A	ASCII string	1		152V
10 Day and Time Convolution of imager with CERES processed (SS4.4)		N/A	ASCII string	1		152V
11 Day and Time TOA and Surface Estimation processed (SS4.5 - 4.6)		N/A	ASCII string	1		152A
12 Number of Footprints in SSF product		N/A	0.. 245475	1		32A
SSF_Record						
Footprint Geometry						
Time and Position						
4 Time of observation	4	day	-0.01 ..1.01	1		64A
5 Radius of satellite from center of Earth at observation	5	km	6000..8000	1		64A
6 Colatitude of satellite at observation	6	deg	0..180	1		32A
7 Longitude of satellite at observation	7	deg	0..360	1		32A
8 Colatitude of Sun at observation	8	deg	0..180	1		32A
9 Longitude of Sun at observation	9	deg	0..360	1		32A
10 Colatitude of CERES FOV at TOA	10	deg	0..180	1		32A
11 Longitude of CERES FOV at TOA	11	deg	0..360	1		32A
12 Colatitude of CERES FOV at surface	12	deg	0..180	1		32A
13 Longitude of CERES FOV at surface	13	deg	0..360	1		32A
14 Scan sample number	14	N/A	1..660	1		16A
15 Packet number	15	N/A	0..32767	1		16A
16 Cone angle of CERES FOV at satellite	16	deg	0..90	1		32A
17 Clock angle of CERES FOV at satellite wrt inertial velocity	17	deg	0..360	1		32A
18 Rate of change of cone angle	18	deg sec^{-1}	-100 .. 100	1		32A
19 Rate of change of clock angle	19	deg sec^{-1}	-10 .. 10	1		32A
20 Along-track angle of CERES FOV at TOA	20	deg	0 .. 360	1		32A
21 Cross-track angle of CERES FOV at TOA	21	deg	-90..90	1		32A
22 X component of satellite inertial velocity	22	km sec^{-1}	-10 ..10	1		64A
23 Y component of satellite inertial velocity	23	km sec^{-1}	-10 ..10	1		64A
24 Z component of satellite inertial velocity	24	km sec^{-1}	-10 ..10	1		64A
CERES Viewing Angles						
25 CERES viewing zenith at TOA	25	deg	0 .. 90	1		32A
26 CERES solar zenith at TOA	26	deg	0 .. 180	1		32A
27 CERES relative azimuth at TOA	27	deg	0..360	1		32A
28 CERES viewing azimuth at TOA wrt North	28	deg	0..360	1		32V
Surface_Map Parameters						
29 Altitude of surface above sea level	29	m	-1000 .. 10000	1		32A
30 Surface type index	30	N/A	1 .. 20	8		16A
31 Surface type percent coverage	31	N/A	0 .. 100	8		16A
Scene_Type						
32 CERES SW ADM type for inversion process	32	N/A	0 .. 200	1		16A
33 CERES LW ADM type for inversion process	33	N/A	0 .. 600	1		16A
34 CERES WN ADM type for inversion process	34	N/A	0 .. 600	1		16A
Footprint Radiation						
CERES Filtered Radiances						
35 CERES TOT filtered radiance, upwards	35	W m^{-2} sr^{-1}	0..700	1		32I
36 CERES SW filtered radiance, upwards	36	W m^{-2} sr^{-1}	-10..510	1		32I
37 CERES WN filtered radiance, upwards	37	W m^{-2} sr^{-1}	0..50	1		32I
38 IES quality flags	38	N/A	see Table TBD	1		32A
CERES Unfiltered Radiances						
39 CERES SW radiance, upwards	39	Wm^{-2} sr^{-1}	-10 .. 510	1		32A
40 CERES LW radiance, upwards	40	Wm^{-2} sr^{-1}	0 .. 200	1		32A
41 CERES WN radiance, upwards	41	Wm^{-2} sr^{-1}	0 .. 50	1		32A

Table B-2. Single Satellite Footprint (SSF) Page 2 of 3

TOA and Surface Flux						
	42	CERES SW flux at TOA, upwards	42	Wm^{-2}	0 .. 1400	1	32A
	43	CERES LW flux at TOA, upwards	43	Wm^{-2}	0 .. 500	1	32A
	44	CERES WN flux at TOA, upwards	44	Wm^{-2}	10 .. 400	1	32A
	45	CERES downward SW surface flux, Model A	45	Wm^{-2}	0 .. 1400	1	32A
	46	CERES downward LW surface flux, Model A	46	Wm^{-2}	0 .. 700	1	32A
	47	CERES downward WN surface flux, Model A	47	Wm^{-2}	0 .. 700	1	32A
	48	CERES downward nonWN surface flux, Model A	48	Wm^{-2}	0 .. 700	1	32A
	49	CERES net SW surface flux, Model A	49	Wm^{-2}	0 .. 1400	1	32A
	50	CERES net LW surface flux, Model A	50	Wm^{-2}	-250 .. 50	1	32A
	51	CERES downward SW surface flux, Model B (TBD)	51	Wm^{-2}	0 .. 1400	1	32A
	52	CERES downward LW surface flux, Model B	52	Wm^{-2}	0 .. 700	1	32A
	53	CERES net SW surface flux, Model B (TBD)	53	Wm^{-2}	0 .. 1400	1	32A
	54	CERES net LW surface flux, Model B	54	Wm^{-2}	-250 .. 50	1	32A
	55	CERES spectral reflectivity	55	N/A	0 .. 1	6	32I
	56	CERES broadband surface albedo	56	N/A	0 .. 1	1	32I
	57	CERES LW surface emissivity	57	N/A	0 .. 1	1	32I
	58	CERES WN surface emissivity	58	N/A	0 .. 1	1	32I
	59	Imager-based surface skin temperature	59	K	175 .. 375	1	32I
Full Footprint Area							
	60	Number of imager pixels in CERES FOV	60	N/A	0 .. 9000	1	16A
	61	Imager percent coverage	61	N/A	0..100	1	16A
	62	Precipitable water	62	cm	0.001 .. 10	1	32A
	63	Shadowed pixels percent coverage (TBD)	63	N/A	0 .. 100	1	16A
	64	Notes on general procedure	64	N/A	TBD	1	16A
	65	Notes on Cloud Algorithms	65	N/A	TBD	1	16A
	66	Mean imager viewing zenith over CERES FOV	66	deg	0 .. 90	1	32A
	67	Mean imager relative azimuth over CERES FOV	67	deg	0 .. 360	1	32A
	68	Imager channel identifier	68	N/A	1 .. 20	5	16A
	69	5th percentile of imager radiances over CERES FOV	69	$W\ m^{-2}\ sr^{-1}\ \mu m^{-1}$	TBD	5	32V
	70	Mean of imager radiances over CERES FOV	70	$W\ m^{-2}\ sr^{-1}\ \mu m^{-1}$	TBD	5	32A
	71	95th percentile of imager radiances over CERES FOV	71	$W\ m^{-2}\ sr^{-1}\ \mu m^{-1}$	TBD	5	32V
Clear Footprint Area							
	72	Sunglint percent coverage	72	N/A	0 .. 100	1	16A
	73	Snow/Ice percent coverage	73	N/A	0 .. 100	1	16A
	74	Smoke percent coverage	74	N/A	0 .. 100	1	16A
	75	Fire percent coverage	75	N/A	0 .. 100	1	16A
	76	Mean of imager radiances over clear area	76	$W\ m^{-2}\ sr^{-1}\ \mu m^{-1}$	TBD	5	32A
	77	Stddev of imager radiances over clear area	77	$W\ m^{-2}\ sr^{-1}\ \mu m^{-1}$	TBD	5	32I
	78	Total aerosol visible optical depth in clear area	78	N/A	0 .. 2	1	32A
	79	Total aerosol effective radius in clear area	79	μm	0 .. 20	1	32A

Table B-3. Single Satellite Footprint (SSF) Page 3 of 3

Cloudy Footprint Area						
Cloud Category Arrays is Array[2] of:						
80	Cloud category area percent coverage	80	N/A	0 .. 100	2	16A
81	Cloud category overcast percent coverage	81	N/A	0 .. 100	2	16A
82	Cloud category broken percent coverage	82	N/A	0 .. 100	2	16A
83	Mean of imager radiances for cloud category	83	W m^{-2} sr^{-1} μm^{-1}	TBD	2 x 5	32A
84	Stddev of imager radiances for cloud category	84	W m^{-2} sr^{-1} μm^{-1}	TBD	2 x 5	32I
85	Mean cloud visible optical depth for cloud category	85	N/A	0 .. 400	2	32A
86	Stddev of visible optical depth for cloud category	86	N/A	TBD	2	32A
87	Mean logarithm of cloud visible optical depth for cloud category	87	N/A	0 .. 6	2	32A
88	Stddev of logarithm of visible optical depth for cloud category	88	N/A	TBD	2	32A
89	Mean cloud infrared emissivity for cloud category	89	N/A	0 .. 1	2	32A
90	Stddev of cloud infrared emissivity for cloud category	90	N/A	TBD	2	32A
91	Mean liquid water path for cloud category	91	g m^{-2}	TBD	2	32A
92	Stddev of liquid water path for cloud category	92	g m^{-2}	TBD	2	32V
93	Mean ice water path for cloud category	93	g m^{-2}	TBD	2	32A
94	Stdev of ice water path for cloud category	94	g m^{-2}	TBD	2	32V
95	Mean cloud top pressure for cloud category	95	hPa	0 .. 1100	2	32A
96	Stddev of cloud top pressure for cloud category	96	hPa	TBD	2	32V
97	Mean cloud effective pressure for cloud category	97	hPa	0 .. 1100	2	32A
98	Stddev of cloud effective pressure for cloud category	98	hPa	TBD	2	32A
99	Mean cloud effective temperature for cloud category	99	K	100 .. 350	2	32A
100	Stddev of cloud effective temperature for cloud category	100	K	TBD	2	32A
101	Mean cloud effective height for cloud category	101	km	0 .. 20	2	32A
102	Stddev of cloud effective height for cloud category	102	km	TBD	2	32V
103	Mean cloud bottom pressure for cloud category	103	hPa	0 .. 1100	2	32A
104	Stddev of cloud bottom pressure for cloud category	104	hPa	TBD	2	32V
105	Mean water particle radius for cloud category	105	µm	TBD	2	32A
106	Stddev of water particle radius for cloud category	106	µm	TBD	2	32A
107	Mean ice particle effective diameter for cloud category	107	µm	TBD	2	32A
108	Stddev of ice particle effective diameter for cloud category	108	µm	TBD	2	32A
109	Mean cloud particle phase for cloud category	109	N/A	0 .. 1	2	32A
110	Stddev of cloud particle phase for cloud category	110	N/A	0 .. 1	2	32V
111	Mean vertical aspect ratio for cloud category (TBD)	111	N/A	0 .. 1	2	32A
112	Stddev of vertical aspect ratio for cloud category (TBD)	112	N/A	TBD	2	32V
113	Percentiles of visible optical depth for cloud category	113	N/A	TBD	2 x 13	32I
114	Percentiles of IR emissivity for cloud category	114	N/A	TBD	2 x 13	32I
Overlap Footprint Area						
115	Number of imager pixels for overlap condition	115	N/A	0 .. 9000	4	16A
116	Overlap condition weighted area percentage	116	N/A	0 .. 100	4	16A

Total Meta Bits/File:	1704
Total Data Bits/Record:	**7744**
Total Records/File:	245475
Total Data Bits/File:	**1900958400**
Total MegaBytes / Hour	237.6
Total GigaBytes / Day	5.7

Appendix C - Nomenclature

Acronyms

ADEOS	Advanced Earth Observing System
ADM	Angular Distribution Model
AIRS	Atmospheric Infrared Sounder (EOS-AM)
AMSU	Advanced Microwave Sounding Unit (EOS-PM)
APD	Aerosol Profile Data
APID	Application Identifier
ARESE	ARM Enhanced Shortwave Experiment
ARM	Atmospheric Radiation Measurement
ASOS	Automated Surface Observing Sites
ASTER	Advanced Spaceborne Thermal Emission and Reflection Radiometer
ASTEX	Atlantic Stratocumulus Transition Experiment
ASTR	Atmospheric Structures
ATBD	Algorithm Theoretical Basis Document
AVG	Monthly Regional, Average Radiative Fluxes and Clouds (CERES Archival Data Product)
AVHRR	Advanced Very High Resolution Radiometer
BDS	Bidirectional Scan (CERES Archival Data Product)
BRIE	Best Regional Integral Estimate
BSRN	Baseline Surface Radiation Network
BTD	Brightness Temperature Difference(s)
CCD	Charge Coupled Device
CCSDS	Consultative Committee for Space Data Systems
CEPEX	Central Equatorial Pacific Experiment
CERES	Clouds and the Earth’s Radiant Energy System
CID	Cloud Imager Data
CLAVR	Clouds from AVHRR
CLS	Constrained Least Squares
COPRS	Cloud Optical Property Retrieval System
CPR	Cloud Profiling Radar
CRH	Clear Reflectance, Temperature History (CERES Archival Data Product)
CRS	Single Satellite CERES Footprint, Radiative Fluxes and Clouds (CERES Archival Data Product)
DAAC	Distributed Active Archive Center
DAC	Digital-Analog Converter
DAO	Data Assimilation Office
DB	Database
DFD	Data Flow Diagram

DLF	Downward Longwave Flux
DMSP	Defense Meteorological Satellite Program
EADM	ERBE-Like Albedo Directional Model (CERES Input Data Product)
ECA	Earth Central Angle
ECLIPS	Experimental Cloud Lidar Pilot Study
ECMWF	European Centre for Medium-Range Weather Forecasts
EDDB	ERBE-Like Daily Data Base (CERES Archival Data Product)
EID9	ERBE-Like Internal Data Product 9 (CERES Internal Data Product)
EOS	Earth Observing System
EOSDIS	Earth Observing System Data Information System
EOS-AM	EOS Morning Crossing Mission
EOS-PM	EOS Afternoon Crossing Mission
ENSO	El Niño/Southern Oscillation
ENVISAT	Environmental Satellite
EPHANC	Ephemeris and Ancillary (CERES Input Data Product)
ERB	Earth Radiation Budget
ERBE	Earth Radiation Budget Experiment
ERBS	Earth Radiation Budget Satellite
ESA	European Space Agency
ES4	ERBE-Like S4 Data Product (CERES Archival Data Product)
ES4G	ERBE-Like S4G Data Product (CERES Archival Data Product)
ES8	ERBE-Like S8 Data Product (CERES Archival Data Product)
ES9	ERBE-Like S9 Data Product (CERES Archival Data Product)
FLOP	Floating Point Operation
FIRE	First ISCCP Regional Experiment
FIRE II IFO	First ISCCP Regional Experiment II Intensive Field Observations
FOV	Field of View
FSW	Hourly Gridded Single Satellite Fluxes and Clouds (CERES Archival Data Product)
FTM	Functional Test Model
GAC	Global Area Coverage (AVHRR data mode)
GAP	Gridded Atmospheric Product (CERES Input Data Product)
GCIP	GEWEX Continental-Phase International Project
GCM	General Circulation Model
GEBA	Global Energy Balance Archive
GEO	ISSCP Radiances (CERES Input Data Product)
GEWEX	Global Energy and Water Cycle Experiment
GLAS	Geoscience Laser Altimetry System
GMS	Geostationary Meteorological Satellite
GOES	Geostationary Operational Environmental Satellite

HBTM	Hybrid Bispectral Threshold Method
HIRS	High-Resolution Infrared Radiation Sounder
HIS	High-Resolution Interferometer Sounder
ICM	Internal Calibration Module
ICRCCM	Intercomparison of Radiation Codes in Climate Models
ID	Identification
IEEE	Institute of Electrical and Electronics Engineers
IES	Instrument Earth Scans (CERES Internal Data Product)
IFO	Intensive Field Observation
INSAT	Indian Satellite
IOP	Intensive Observing Period
IR	Infrared
IRIS	Infrared Interferometer Spectrometer
ISCCP	International Satellite Cloud Climatology Project
ISS	Integrated Sounding System
IWP	Ice Water Path
LAC	Local Area Coverage (AVHRR data mode)
LaRC	Langley Research Center
LBC	Laser Beam Ceilometer
LBTM	Layer Bispectral Threshold Method
Lidar	Light Detection and Ranging
LITE	Lidar In-Space Technology Experiment
Lowtran 7	Low-Resolution Transmittance (Radiative Transfer Code)
LW	Longwave
LWP	Liquid Water Path
MAM	Mirror Attenuator Mosaic
MC	Mostly Cloudy
MCR	Microwave Cloud Radiometer
METEOSAT	Meteorological Operational Satellite (European)
METSAT	Meteorological Satellite
MFLOP	Million FLOP
MIMR	Multifrequency Imaging Microwave Radiometer
MISR	Multiangle Imaging Spectroradiometer
MLE	Maximum Likelihood Estimate
MOA	Meteorology Ozone and Aerosol
MODIS	Moderate-Resolution Imaging Spectroradiometer
MSMR	Multispectral, multiresolution
MTSA	Monthly Time and Space Averaging
MWH	Microwave Humidity

MWP	Microwave Water Path
NASA	National Aeronautics and Space Administration
NCAR	National Center for Atmospheric Research
NCEP	National Centers for Environmental Prediction
NESDIS	National Environmental Satellite, Data, and Information Service
NIR	Near Infrared
NMC	National Meteorological Center
NOAA	National Oceanic and Atmospheric Administration
NWP	Numerical Weather Prediction
OLR	Outgoing Longwave Radiation
OPD	Ozone Profile Data (CERES Input Data Product)
OV	Overcast
PC	Partly Cloudy
POLDER	Polarization of Directionality of Earth's Reflectances
PRT	Platinum Resistance Thermometer
PSF	Point Spread Function
PW	Precipitable Water
RAPS	Rotating Azimuth Plane Scan
RPM	Radiance Pairs Method
RTM	Radiometer Test Model
SAB	Sorting by Angular Bins
SAGE	Stratospheric Aerosol and Gas Experiment
SARB	Surface and Atmospheric Radiation Budget Working Group
SDCD	Solar Distance Correction and Declination
SFC	Hourly Gridded Single Satellite TOA and Surface Fluxes (CERES Archival Data Product)
SHEBA	Surface Heat Budget in the Arctic
SPECTRE	Spectral Radiance Experiment
SRB	Surface Radiation Budget
SRBAVG	Surface Radiation Budget Average (CERES Archival Data Product)
SSF	Single Satellite CERES Footprint TOA and Surface Fluxes, Clouds
SSMI	Special Sensor Microwave Imager
SST	Sea Surface Temperature
SURFMAP	Surface Properties and Maps (CERES Input Product)
SW	Shortwave
SWICS	Shortwave Internal Calibration Source
SYN	Synoptic Radiative Fluxes and Clouds (CERES Archival Data Product)
SZA	Solar Zenith Angle
THIR	Temperature/Humidity Infrared Radiometer (Nimbus)

TIROS	Television Infrared Observation Satellite
TISA	Time Interpolation and Spatial Averaging Working Group
TMI	TRMM Microwave Imager
TOA	Top of the Atmosphere
TOGA	Tropical Ocean Global Atmosphere
TOMS	Total Ozone Mapping Spectrometer
TOVS	TIROS Operational Vertical Sounder
TRMM	Tropical Rainfall Measuring Mission
TSA	Time-Space Averaging
UAV	Unmanned Aerospace Vehicle
UT	Universal Time
UTC	Universal Time Code
VAS	VISSR Atmospheric Sounder (GOES)
VIRS	Visible Infrared Scanner
VISSR	Visible and Infrared Spin Scan Radiometer
WCRP	World Climate Research Program
WG	Working Group
Win	Window
WN	Window
WMO	World Meteorological Organization
ZAVG	Monthly Zonal and Global Average Radiative Fluxes and Clouds (CERES Archival Data Product)

Symbols

A	atmospheric absorptance
$B_\lambda(T)$	Planck function
C	cloud fractional area coverage
CF_2Cl_2	dichlorofluorocarbon
$CFCl_3$	trichlorofluorocarbon
CH_4	methane
CO_2	carbon dioxide
D	total number of days in the month
D_e	cloud particle equivalent diameter (for ice clouds)
E_o	solar constant or solar irradiance
F	flux
f	fraction
G_a	atmospheric greenhouse effect
g	cloud asymmetry parameter
H_2O	water vapor

I	radiance
i	scene type
m_i	imaginary refractive index
$\hat{N}$	angular momentum vector
N_2O	nitrous oxide
O_3	ozone
P	point spread function
p	pressure
Q_a	absorption efficiency
Q_e	extinction efficiency
Q_s	scattering efficiency
R	anisotropic reflectance factor
r_E	radius of the Earth
r_e	effective cloud droplet radius (for water clouds)
r_h	column-averaged relative humidity
S_o	summed solar incident SW flux
S_o'	integrated solar incident SW flux
T	temperature
T_B	blackbody temperature
t	time or transmittance
W_{liq}	liquid water path
w	precipitable water
$\hat{x}_o$	satellite position at t_o
x, y, z	satellite position vector components
$\dot{x}, \dot{y}, \dot{z}$	satellite velocity vector components
z	altitude
z_{top}	altitude at top of atmosphere
α	albedo or cone angle
β	cross-scan angle
γ	Earth central angle
γ_{at}	along-track angle
γ_{ct}	cross-track angle
δ	along-scan angle
ε	emittance
Θ	colatitude of satellite
θ	viewing zenith angle
θ_o	solar zenith angle
λ	wavelength
μ	viewing zenith angle cosine

μ_o	solar zenith angle cosine
ν	wave number
ρ	bidirectional reflectance
τ	optical depth
$\tau_{aer}(p)$	spectral optical depth profiles of aerosols
$\tau_{H_2O\lambda}(p)$	spectral optical depth profiles of water vapor
$\tau_{O_3}(p)$	spectral optical depth profiles of ozone
Φ	longitude of satellite
ϕ	azimuth angle
$\tilde{\omega}_o$	single-scattering albedo

Subscripts:

c	cloud
cb	cloud base
ce	cloud effective
cld	cloud
cs	clear sky
ct	cloud top
ice	ice water
lc	lower cloud
liq	liquid water
s	surface
uc	upper cloud
λ	spectral wavelength

Units

AU	astronomical unit
cm	centimeter
cm-sec^{-1}	centimeter per second
count	count
day	day, Julian date
deg	degree
deg-sec^{-1}	degree per second
DU	Dobson unit
erg-sec^{-1}	erg per second
fraction	fraction (range of 0–1)
g	gram
g-cm^{-2}	gram per square centimeter
g-g^{-1}	gram per gram
g-m^{-2}	gram per square meter

h	hour
hPa	hectopascal
K	Kelvin
kg	kilogram
$kg\text{-}m^{-2}$	kilogram per square meter
km	kilometer
$km\text{-}sec^{-1}$	kilometer per second
m	meter
mm	millimeter
μm	micrometer, micron
N/A	not applicable, none, unitless, dimensionless
$ohm\text{-}cm^{-1}$	ohm per centimeter
percent	percent (range of 0–100)
rad	radian
$rad\text{-}sec^{-1}$	radian per second
sec	second
sr^{-1}	per steradian
W	watt
$W\text{-}m^{-2}$	watt per square meter
$W\text{-}m^{-2}sr^{-1}$	watt per square meter per steradian
$W\text{-}m^{-2}sr^{-1}\mu m^{-1}$	watt per square meter per steradian per micrometer